SANDIA REPORT
SAND2011-0899
Unlimited Release
Printed February 2011

Programmed Assembly of Nanoscale Structures using Peptoids

David B. Robinson, George M. Buffleben, Michael S. Kent, Rex P. Hjelm, Kiran Morishetti, Scott Russell, Jianhua Ren, and Ronald N. Zuckermann

Prepared by
Sandia National Laboratories
Albuquerque, New Mexico 87185 and Livermore, California 94550

Sandia National Laboratories is a multi-program laboratory managed and operated by Sandia Corporation, a wholly owned subsidiary of Lockheed Martin Corporation, for the U.S. Department of Energy's National Nuclear Security Administration under contract DE-AC04-94AL85000.

Issued by Sandia National Laboratories, operated for the United States Department of Energy by Sandia Corporation.

SAND2011-0899
Unlimited Release
Printed February 2011

Programmed Assembly of Nanoscale Structures using Peptoids

David B. Robinson[1], George M. Buffleben[2], Michael S. Kent[3], Rex P. Hjelm[4], Kiran Morishetti[5], Scott Russell[6], Jianhua Ren[5], and Ronald N. Zuckermann[7]

(1) Energy Nanomaterials Department; (2) Systems Biology Department
Sandia National Laboratories
P.O. Box 969
Livermore, California 94551-MS9291

(3) Bioenergy and Defense Technologies
Sandia National Laboratories
P.O. Box 5800
Albuquerque, New Mexico 87185-MS1349

(4) Lujan Neutron Scattering Center
Los Alamos National Laboratory
Los Alamos, New Mexico 87545

(5) Department of Chemistry
University of the Pacific
3601 Pacific Avenue
Stockton, California 95211

(6) Department of Chemistry
California State University, Stanislaus
Turlock, California 95382

(7) Molecular Foundry
Lawrence Berkeley National Laboratory
1 Cyclotron Road Mail Stop 67R5110
Berkeley, California 94720

Abstract

Sequence-specific polymers are the basis of the most promising approaches to bottom-up programmed assembly of nanoscale materials. Examples include artificial peptides and nucleic acids. Another class is oligo(N-functional glycine)s, also known as peptoids, which permit greater sidegroup diversity and conformational control, and can be easier to synthesize and purify. We have developed a set of peptoids that can be used to make inorganic nanoparticles more compatible with biological sequence-specific polymers so that they can be incorporated into nucleic acid or other biologically based nanostructures. Peptoids offer degrees of modularity, versatility, and predictability that equal or exceed other sequence-specific polymers, allowing for rational design of oligomers for a specific purpose. This degree of control will be essential to the development of arbitrarily designed nanoscale structures.

ACKNOWLEDGMENTS

Portions of this work were performed at the Molecular Foundry, Lawrence Berkeley National Laboratory, which is supported by the Office of Science, Office of Basic Energy Sciences, U.S. Department of Energy, under Contract No. DE-AC02-05CH11231.

We thank Michael Connolly and Byoung-Chul Lee at the Molecular Foundry, as well as other Foundry users and staff, for their assistance in the art of peptoid synthesis and purification.

CONTENTS

FIGURES

1. GOAL

Photolithography, the prevalent technology for formation of nanoscale structures, is difficult and expensive on length scales below 100 nm because in this regime it becomes increasingly difficult to manipulate the light used to modify photosensitive materials. This method is unlikely to achieve widespread use for fabrication of structures with sub-20 nm features. A fundamentally new technology must be developed to create structures smaller than 20 nm that can be integrated with a photolithographic process without hindering throughput. Furthermore, photolithography uses two-dimensional patterns; in the vertical direction, the process must be iterated. The powerful parallelism achieved in the other two dimensions is absent.

Sandia and many other research institutions have made great efforts toward the synthesis of nanowires and nanoparticles, with the hope that they will lead to electronic circuits beyond the limits of photolithography, to new electronic and optical transducers, memory elements, and other devices that exploit quantum confinement effects, and analytical devices that interface with single molecules or enzymes. Some methods are known for assembling nanomaterials into ordered arrays.[1] However, relatively little effort or progress has been made toward the arbitrary and scalable arrangement of these materials into useful, rigid structures. In other words, we have many lumber mills, and we can stack wood into piles, but nobody has invented nails yet.

Achievement of precise three-dimensional (3D) control below 20 nm is best obtained through the highly selective affinity of sequence-specific synthetic macromolecules that act as scaffolding for functional inorganic materials. These macromolecules are to assemble into a prescribed 3D structure and direct the deposition of inorganic material at specific locations within that framework. This directed assembly is known to occur in living organisms using polypeptides. Unfortunately, these materials and their design rules are too complex to be within reach of an artificial application.

Deoxyribonucleic acid (DNA) can provide specific connectivity and long-range chirality, and has been used to create elaborate 3D nanostructures.[2] However, DNA alone is too flexible, sensitive to environmental conditions, and limited in monomer functionality. It has thus proven difficult to use as templates for precisely positioned inorganic material.

The largest body of work on programmable supramolecular assemblies involves modification of protein assemblies.[3-5] This work, while promising, suffers from the limitations mentioned above: they require specific aqueous salt solutions and temperature conditions, and do not permit systematic design of new architectures due to their complexity. Smaller molecules can also form supramolecular assemblies,[6] but afford little sophistication or control over changes in position or orientation on the 1–50 nm scale necessary for 3D control.

Many have used peptide assemblies to template inorganic materials, most notably using m13 bacteriophage coat proteins.[7] Regulated growth using this technique is a challenge because material is only coated on the outside of the structure, and complex morphologies cannot be programmed. Only simple wires have been demonstrated using this method. Growth has been demonstrated in the interior of organic[8] and inorganic[9] pores of fixed geometry. More

commonly, nanostructured inorganic materials are synthesized using surfactant templates.[10,11] This approach results in rough control over average size, shape, and spacing of simple features such as cylindrical or tortuous pores. Oriented alignment of complex structures onto a substrate is of major academic and commercial interest, but work has primarily involved much larger length scales[12] or periodic arrays.[1]

To provide rigidity, chemical stability, and specific interactions with inorganic materials, we seek to interface DNA with oligo (N-functional glycine)s (NFG or "peptoids"). These short polymers can be designed to have helical conformations that are stable under extreme conditions and allow precise positioning of chemical functionality. Inorganic material can then be connected with DNA templates with these, using a combination of peptoids on the particle or the DNA structure that provide physical and chemical protection and specificity, or inorganic material can be grown on a peptoid template. In this project, we have evaluated each of these approaches, and have focused on the use of peptoids to make inorganic particles more compatible with DNA templating technology.

Poly(N-functionalized glycine)s, with 15 years of development,[13] are well characterized and easily synthesized with high molecular weight and yield. When chiral side chains are used, they form helical rod conformations that are stable under a wide range of solvent conditions and temperatures. Side-chain functional groups can be incorporated without disrupting the overall conformation, which can be used to interact with inorganic materials. Methods for making branched structures are also under development. Stable, specific helical bundles with designed inter- and supramolecular interactions have been synthesized by combinatorial methods,[14] and further stabilized by covalent crosslinking.[15] These polymers and their supramolecular assemblies are a major focus of study at Lawrence Berkeley Lab's DOE-funded Molecular Foundry, and Sandia has been involved in these efforts through this project. We have developed these materials to encapsulate inorganic materials and assemble them into simple test structures of controlled geometry, as required in nanoscale electronic, optical or fluidic circuitry.

The use of peptoids bypasses many disadvantages that plague other attempts to gain architectural control over the 1–50 nm scale. The simplicity, stability, and diverse chemical functionality of chiral oligo(N-substituted glycines) makes them a robust platform for rational and systematic development of inorganic materials templated by their assemblies. This provides the freedom to generate materials that are sophisticated enough to behave in specific, designed ways, while remaining simple enough to be predictable — a balance that has previously been absent. Our approach will eventually permit the synthesis of inorganic nanomaterials with an entirely new class of structure and functionality, as well as their integration into device structures that have otherwise been difficult or uneconomical to achieve. Templating through sequence-specific polymers is a fundamental approach to material synthesis that is likely to be to the 21st century what photolithography was to the 20th century.

2. ARTIFICIAL POLYMERS MIMIC BACTERIOPHAGE CAPSID PROTEINS TO PROTECT AND FUNCTIONALIZE NUCLEIC ACID STRUCTURES

This chapter has been submitted for publication as a book chapter in the American Chemical Society Symposium Series.

2.1. Abstract

The filamentous bacteriophage m13 and related viruses encapsulate DNA with protein, forming an organic nanowire about 1 micrometer long and less than 10 nanometers wide. The length of the wire is formed from many copies of a single protein, which is a single alpha helix formed from about 50 amino acids. It can be viewed as a very sophisticated surfactant, with hydrophilic regions that interact with the DNA and form the outer surface, and hydrophobic regions that pack against each other. We have implemented these design principles in peptoids (sequence-specific N-functional glycine oligomers) and have found that they form aggregates with DNA that have adjustable properties. This approach may complement phage display methods, providing new approaches to gene transfection and nanofabrication that do not require expression in bacteria and that provide a wider range of chemical stability and functionality.

2.2. Introduction

Surfactants are central to the control of size, shape, and assembly of nanoscale materials in both artificial and living systems. State-of-art inorganic nanoparticles are synthesized using readily available surfactants such as oleic acid, oleylamine, hexadecyltrimethylammonium bromide, and trialkyl phosphine oxides. By adjusting the relative concentrations of these, nearly monodisperse particles of metals, metal oxides, or II-VI semiconductors can be made as spheres or similar low aspect ratio shapes in the 2-20 nm range.[16] At higher ratios of surfactant to metal precursor, ordered assembly of surfactants and/or association of surfactants with specific crystal faces allows formation of materials with higher aspect ratio.[17,18] At very high concentrations, some surfactants form lyotropic liquid crystal phases that can serve as templates for porous materials.[19]

Much more exquisite structural control is obtained in living systems, the simplest of which are viruses, which can be precisely monodisperse. Two well known examples of high aspect ratio are tobacco mosaic virus[20,21] and the filamentous bacteriophage family, the most studied of which is m13.[22,23] This control is achieved through the use of two types of sequence-specific polymers or oligomers: nucleic acids that act as templates for assembly, and peptides or proteins with precisely located hydrophilic and hydrophobic regions defined through their sequence and conformation, as well as additional chemical functionality, that assemble onto this template. This scheme can inspire strategies toward development of more sophisticated artificial nanostructured materials. Control of material on this scale is of known value for information storage,[24] interfacing with biological systems for diagnosis and therapy,[25] and energy storage and harvesting,[26,27] among other applications.

Substantial efforts have been made to modify viruses to make them useful for these applications. Chemical modification of intact viruses has allowed growth of inorganic materials in or around them.[28,29] Other chemical modifications have been used to create specific biological interactions.[30]

To gain a greater degree of architectural control, it would be valuable to have a detailed understanding of the principles by which the viral particles are constructed. The tobacco mosaic virus can be assembled in vitro by mixing its single-stranded RNA with the 17.5 kDa capsid protein under the proper conditions.[20,31] The capsid grows from both individual proteins and preformed small aggregates or discs. There is a nucleation site within the RNA sequence where a disc of capsid proteins binds. The 5' end is threaded through the center of the disc. Capsid growth is rapid in the 5' direction as entire discs add on that side, whereas growth in the 3' direction involves addition of smaller aggregates or individual proteins and is smaller.

The bacteriophage family has a much smaller major coat protein – a single alpha helix built from about 50 amino acids. The free proteins have low solubility, and their assembly is achieved in a membrane-mediated process within their bacterial hosts.[32,33] When they are assembled, cationic residues near the C terminus are in close proximity to the anionic phosphate backbone of the single-stranded DNA genome, neutral and anionic hydrophilic residues face outward toward the aqueous environment, and hydrophobic residues are buried within neighboring coat proteins. The structure of one of the coat proteins as recorded in the Protein Data Bank (1IFP) is shown in Figure 2-1.

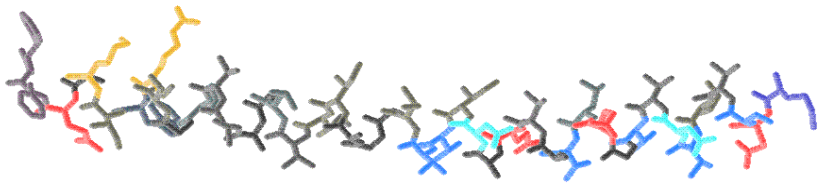

Figure 2-1. pf3 major capsid protein structure from the Protein Data Bank, with hydrophobic residues colored gray, cationic residues yellow, anionic residues red, and neutral hydrophilic functionality in shades of blue.

The sequence of the protein is easily modified by biological techniques, and substantial virion yields are still possible when major changes are made to some or all of the proteins in a particle.[34] The structure and assembly principles of this protein are simple enough that they present a useful starting point for design of artificial polymers that test the generality of this approach to encapsulation of nucleic acids, and for development of molecules that combine the well defined structure and robust aqueous stability of the viruses with the convenience, scalability, and functionality afforded by artificial chemical synthesis.

Our proposed strategy is to synthesize sequence-specific oligomers that are known to adopt well defined helical conformations. If the conformation is known, then functionality can be introduced at well defined and known relative positions along the backbone. Peptide oligomers are known to adopt such conformations, relying on hydrogen bonding within the backbone to

achieve helicity.[35] Another approach is known that does not rely on hydrogen bonding, and is thus insensitive to agents that disrupt it, as well as to enzymes that can degrade proteins. This is a class of peptoids (peptide mimics) in which functionality appears on the amide nitrogen instead of the alpha carbon.[13,36] Such N-functional glycine oligomers rely on the use of bulky chiral side groups to establish helical conformations that are stable even in 8M aqueous urea at 75 C.[37]

2.3. Synthesis of Peptoids

The peptoids are synthesized on a Rink amide resin solid support. A terminal bromoacetamide group is formed by coupling bromoacetic acid to a terminal primary or secondary amine using one equivalent of diisopropylcarbodiimide (DIC) in dimethyl formamide (DMF) at room temperature for a few minutes. After rinsing with DMF, a primary amine dissolved in DMF is added, which displaces the bromide to form a terminal secondary amine in about one hour at room temperature. After rinsing, these steps repeat for each monomer in the desired sequence, as shown in Figure 2-2. The process can be automated by using a low-cost programmable syringe pump with an 8-port valve to feed reagents to a septum-capped fritted reaction tube containing the resin. Three two-way solenoid valves provide agitation by bubbling the solution with nitrogen, and drain spent reactants and rinsate to a waste container. Figures 2-3 and 2-4 are photographs of one version of such an apparatus. A 5 psi nitrogen relief valve is included. Reagents are stored in 50 mL centrifuge tubes with tubing passing through the caps (not an airtight seal). Reagents enter the reaction tube through a crimped needle that sprays reagents downward into the reaction tube.

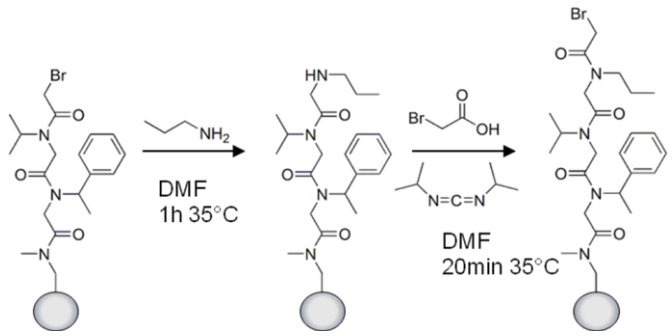

Figure 2-2. Reaction scheme for synthesis of N-functional glycine oligomers on a solid support.

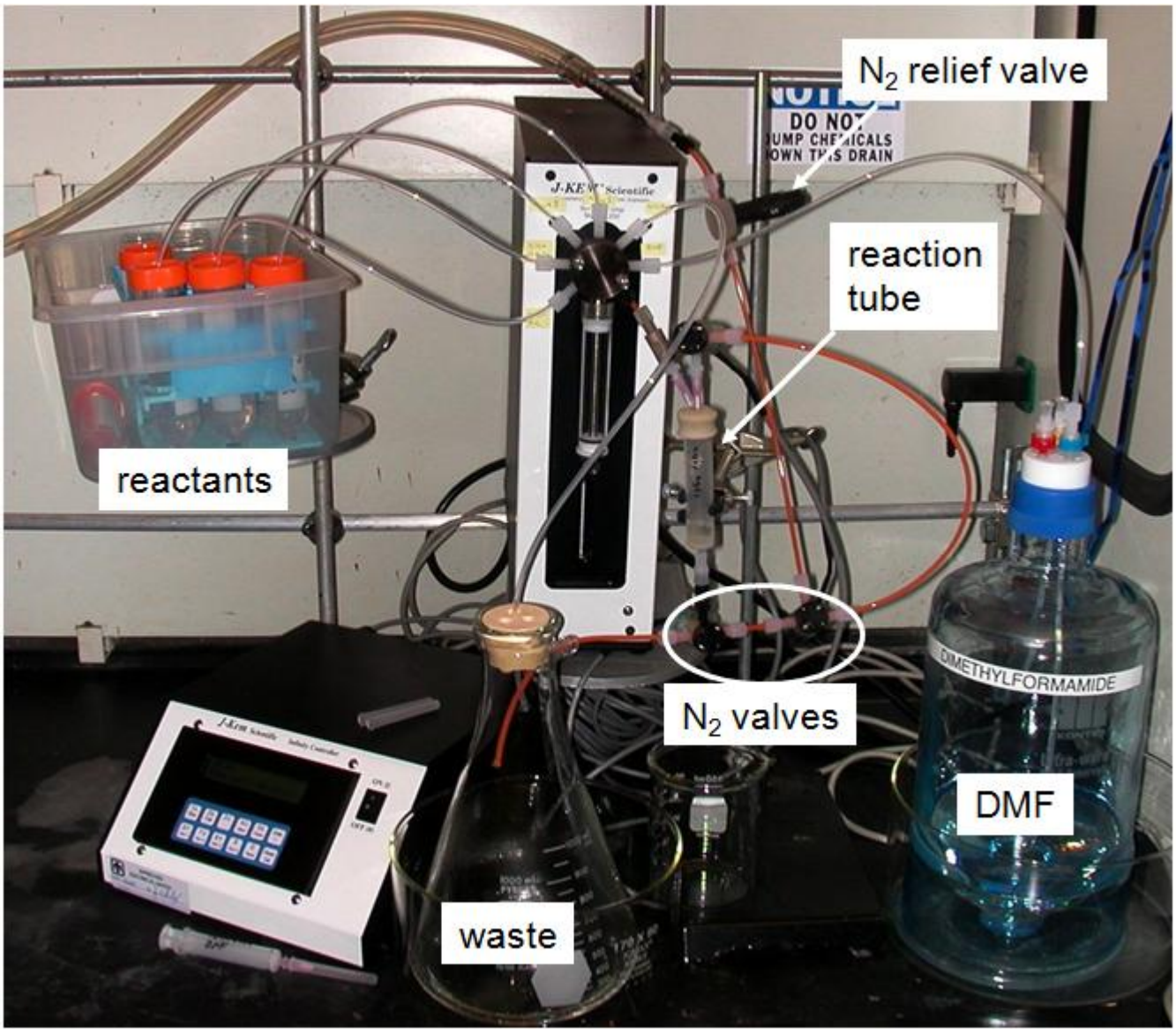

Figure 2-3. Peptoid synthesizer that uses a programmable syringe pump (J-Kem) and valve assembly to dispense reagents and solvent to a fritted reaction tube.

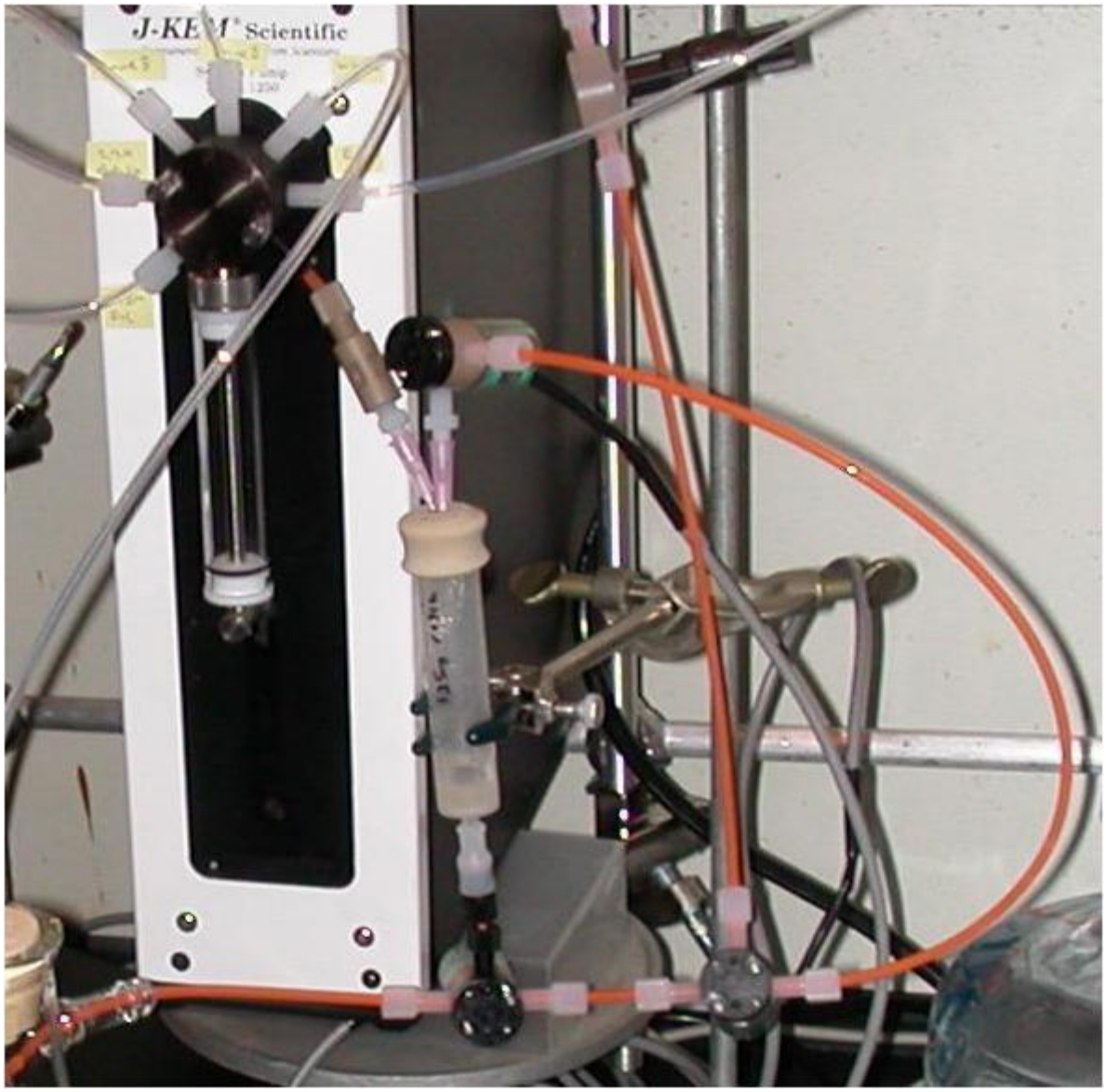

Figure 2-4. Closer view of syringe pump, reaction tube, and valves.

A range of bulky chiral primary amines is available commercially, most notably from BASF, and from Chem-Impex for a range of amines with protected functional groups. The sidegroups that have been most carefully studied for establishment of helical conformations are the hydrophobic α-methyl benzylamines and the t-butyl ester of alanine.[37,38] Protected amines are usually provided as hydrochloride salts, and these must be converted to the free base before use. This is achieved by dissolving or suspending the hydrochloride salt in dichloromethane, adding a nearly stoichiometric amount of 4M potassium hydroxide, and extracting the HCl into the aqueous phase. After separating, the organic phase is washed with brine, dried with magnesium sulfate, and reduced to an oily or waxy product by rotary evaporation. This product is dissolved in DMF or N-methyl pyrrolidone. Amine and bromoacetic acid solutions are typically 0.5M to 1M and the DIC is either neat or 3M. It is advisable to use a slight excess of bromoacetic acid versus

DIC, so care should be taken in determining the molarity of these reagents, but the amine concentration is less critical.

The Rink amide resin initially contains a fluorenylmethyloxycarbonyl (Fmoc)-protected amine bonded to a bis (alkoxyphenyl) methyl group that is in turn tethered to a polystyrene support. Before synthesis, the Fmoc group is removed with 20% 4-methylpiperidine in DMF. At the end, the oligomer is cleaved from the resin using 95:5 trifluoroacetic acid (TFA):water, leaving a primary amide at the C terminus. Any t-butyl ester, t-butoxycarbonyl, or triphenylmethyl protecting groups on sidechains are also removed, but not necessarily with complete generality. The N terminus is protonated by the acid, unless it had been acetylated using either carbodiimide chemistry or a mixture of 0.4M acetic anhydride and 0.4M pyridine in DMF. The crude product is typically redissolved in an acetonitrile-water mixture containing about 0.1% TFA.

The crude product usually contains small amounts of byproducts that are missing a monomer, were incompletely deprotected, or are degraded. For some applications, it may be possible to use the crude product or use a simple purification procedure, but in general, it is necessary to purify the product by preparatory HPLC on a C18 or C4 column using an acetonitrile-water gradient that contains 0.1% TFA. Product fractions are checked using LC-MS or MALDI-MS, concentrated using vacuum centrifugation, and freeze dried.

2.4. Helical Peptoid Surfactants

If in a thought experiment the m13 coat peptide is split in the middle, one obtains two fragments that each have surfactant character. The right half in Figure 2-1 has a longitudinal hydrophobic stripe and a wider longitudinal hydrophilic stripe. This arrangement is similar to the water-soluble helical peptoid studied by Sanborn et al,[37] who denote their sequence as $(NsceNsceNspe)_{12}$. The Nsce monomer has an *S*-1-carboxyethyl sidegroup, and Nspe has an *S*-1-phenylethyl sidegroup. It is believed that helical peptoids adopt a pitch of three monomers per turn,[13] which would align the Nspe monomers longitudinally.

The left half of m13 has a narrow domain of hydrophilic groups approximately on the opposite side, and with opposite charge. Peptoids with similar motifs have been studied as mimics of lung surfactants that are used to treat premature infants.[39] We have synthesized several of this family, of the form $(Nspe_2Nae)_nNspe_2$, where Nae is an aminoethyl sidegroup. Variants have an acetylated N terminus, or diisopropyl aminoethyl sidegroups (Ndipae), or Nrpe, the *R* enantiomer of Nspe. One of these is drawn in Figure 2-5.

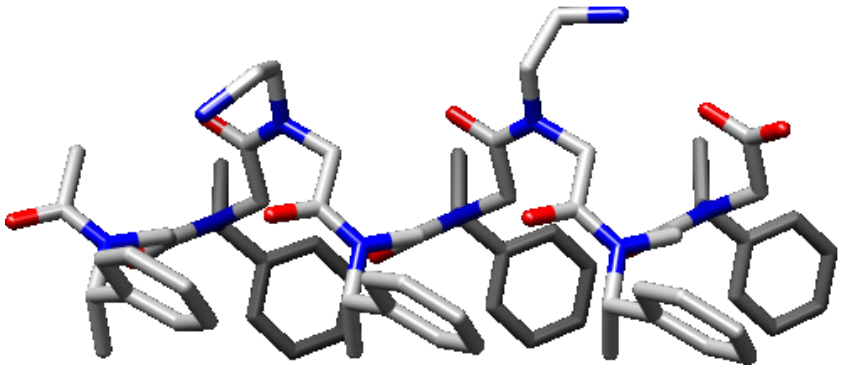

Figure 2-5. Structure of Ac(Nspe$_2$Nae)$_2$Nspe$_2$.

The peptoid (Nspe$_2$Nae)$_3$Nspe$_2$ forms aggregates at 2 mM concentrations in water, as determined from the timescale of the autocorrelation function of the dynamic light scattering signal, as shown in Figure 2-6. The hydrodynamic radius derived from this is 98 nm, but this number is derived assuming a spherical aggregate; a rodlike aggregate can be expected to diffuse slowly and give a radius that is similarly much larger than the length of a single molecule. Figure 2-6 also shows that the peptoid does not aggregate in 2-ethylhexanol. The circular dichroism spectra of Ac(Nrpe$_2$Ndipae)$_2$Nrpe$_2$ was measured in that solvent, showing evidence of a helical conformation: the characteristic pair of peaks above and opposite peak below 200 nm in Figure 2-7.[40,41] Aggregation of this peptoid, which may aid adoption of helical conformations, was observed by light scattering in 2-ethylhexanol.

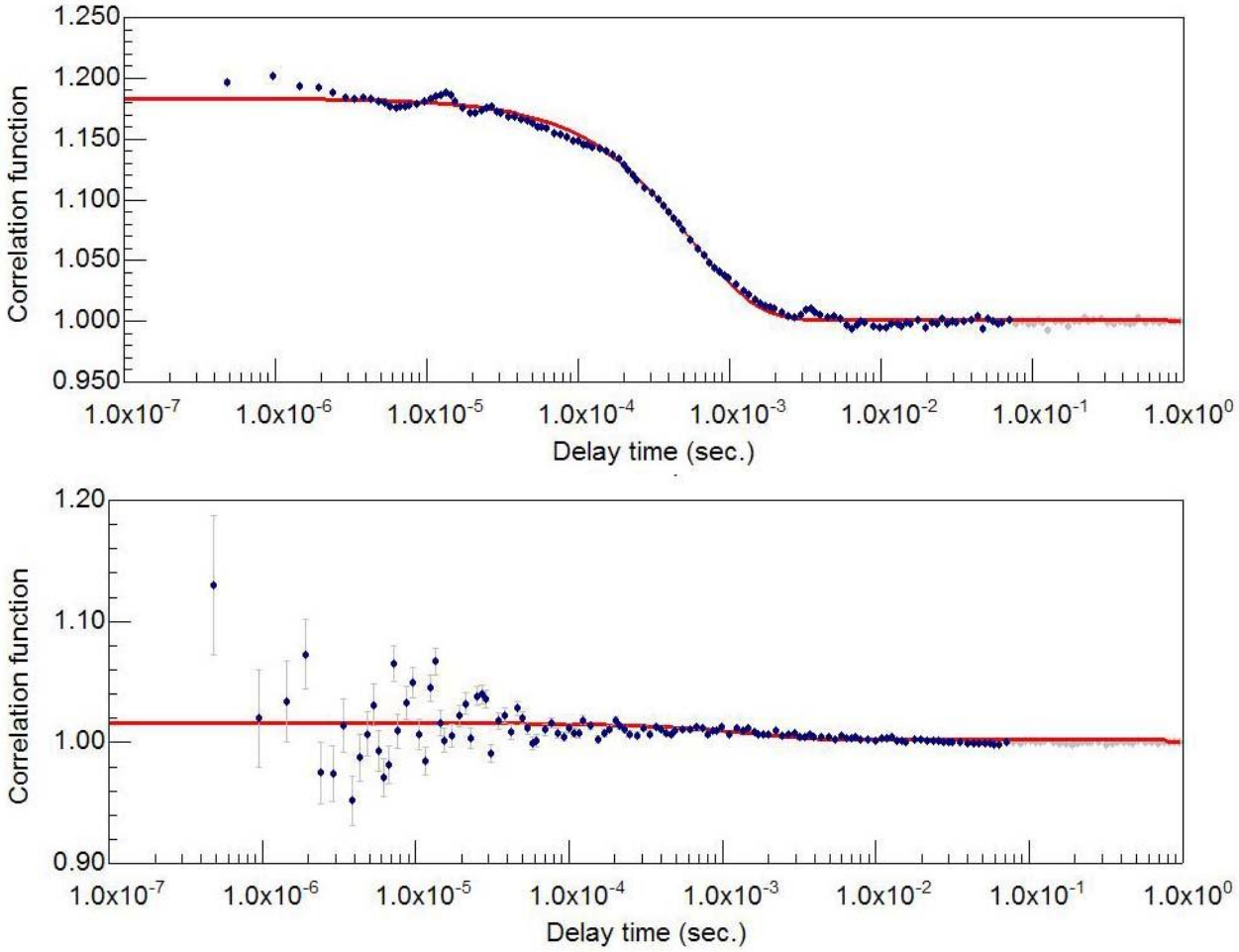

Figure 2-6. Dynamic light scattering correlation functions for $(Nspe_2Nae)_3Nspe_2$ in water (top) and 2-ethylhexanol (bottom).

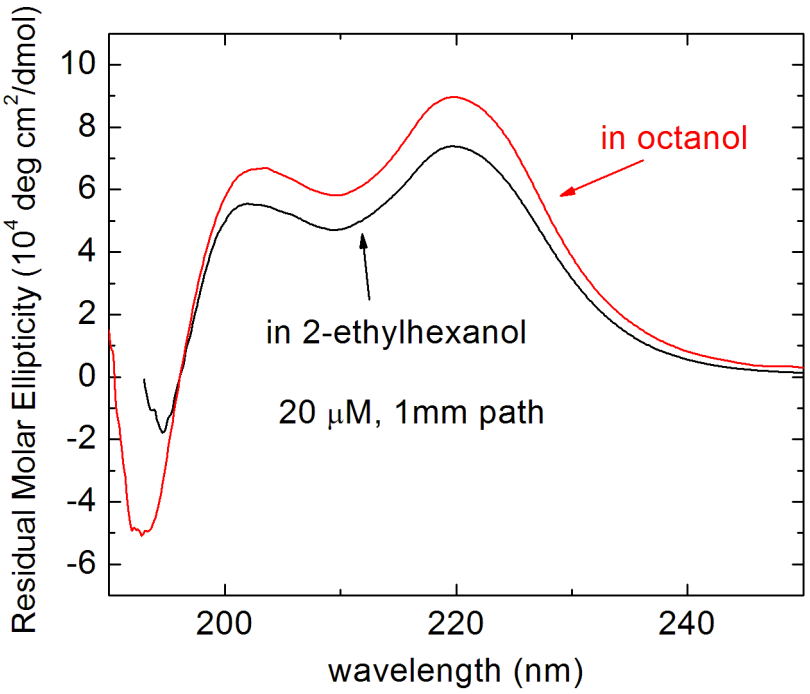

Figure 2-7. Circular dichroism of $Ac(Nrpe_2Ndipae)_2Nrpe_2$ in long-chain alcohols.

2.5. Bacteriophage Mimic Peptoids

To construct an initial peptoid that bears the motifs of the bacteriophage coat protein, we have joined three segments into a sequence: on the N-terminal end, the $(Nspe_2Nae)_x$ segment, an intermediate $Nspe_{3y}$ segment, and a $(NsceNsceNspe)_z$ segment. We designate this series as "Phage xyz", where each of x, y, and z are 1 or 2. These peptoids are much smaller than the phage coat protein, but are water-soluble and easy to synthesize, allowing for initial characterization to ensure that properties are following trends toward those of useful materials. Phage 112 is illustrated in Figure 2-8.

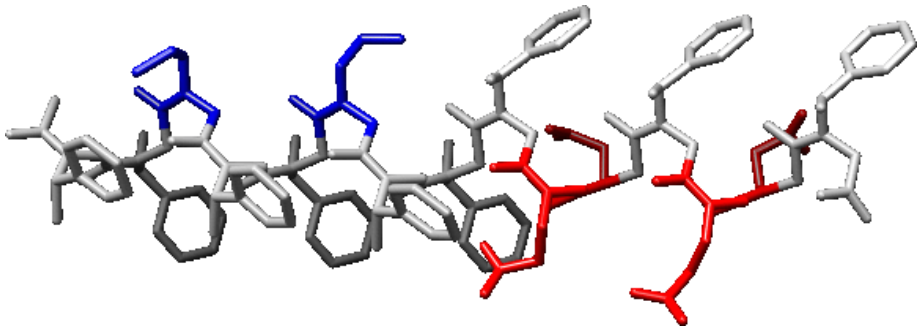

Figure 2-8. Model of phage 112 peptoid, with sequence $(Nspe_2Nae)_1Nspe_3(NsceNsceNspe)_2$

Our goal with this peptoid family is to create an aggregate with nucleic acids that are rigid rodlike and water-soluble. Compact DNA-peptoid aggregates have been previously studied for gene transfection applications.[42,43] Rodlike structures may prove useful for this application, and also may help stabilize DNA origami and related structures under a broader range of solution conditions without inducing a disordered structure.[44-46]

To evaluate the performance of phage 212 and phage 112, the peptoids were combined with double-stranded DNA ladders (about 4 peptoid molecules per DNA base) and run through a 0.8% agarose electrophoresis gel in TAE buffer. The peptoids showed no interaction with DNA at pH 7, as shown in the images of fluorescence of ethidium bromide intercalated with DNA. However, after reducing the pH with acetic acid or hydrochloric acid so that the carboxyl groups were partially protonated, phage 212 formed an aggregate with DNA, whereas phage 112 did not. Coomassie staining of the peptoids (Invitrogen SimplyBlue SafeStain) after capturing the fluorescence image shows that phage 112 still has a net negative charge under the more acidic conditions, traveling in the same direction as the DNA, but decreasing due to the pH reduction. The phage 212-DNA aggregate did not stain or did not stay in the gel during the staining procedure.

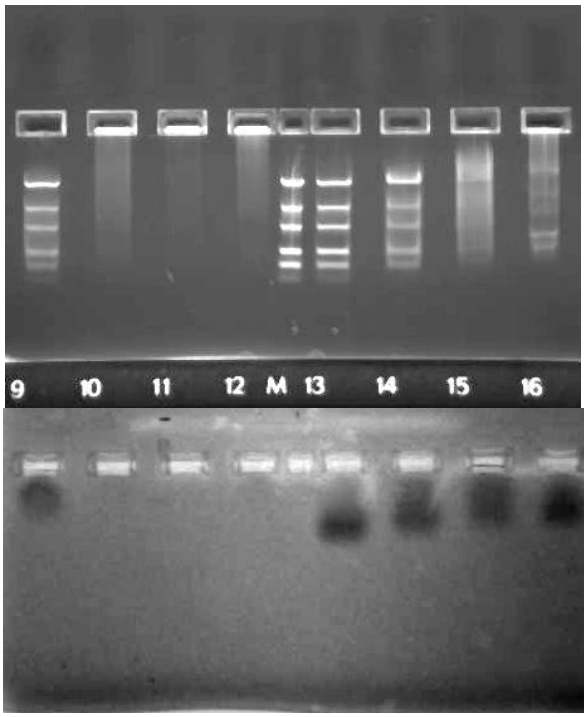

Figure 2-9. 0.8% Agarose gel electrophoresis of peptoid-DNA ladder mixtures in TAE buffer. The top image shows fluorescence of ethidium bromide bound to double-stranded DNA. The bottom image shows Coomassie-stained peptoids. The left 4 lanes are with Phage 212, and the right 4 are with Phage 112. For these, pH decreases from left to right. The center lane contains only the DNA ladder.

As with the simpler cationic surfactants, the phage mimics form aggregates in aqueous solution, as shown in Figure 2-10 for phage 112. The derived hydrodynamic radius of 36 nm is greater than the length scale of an individual peptoid molecule. This is corroborated by transmission electron microscopy of grids that were dipped into this solution. A drop of 1% sodium tungstosilicate (pH between 7 and 8) was placed on the grid and then wicked off, acting as a negative stain. Figure 2-11 shows partially filamentous structures that are larger when the peptoid and DNA are combined.

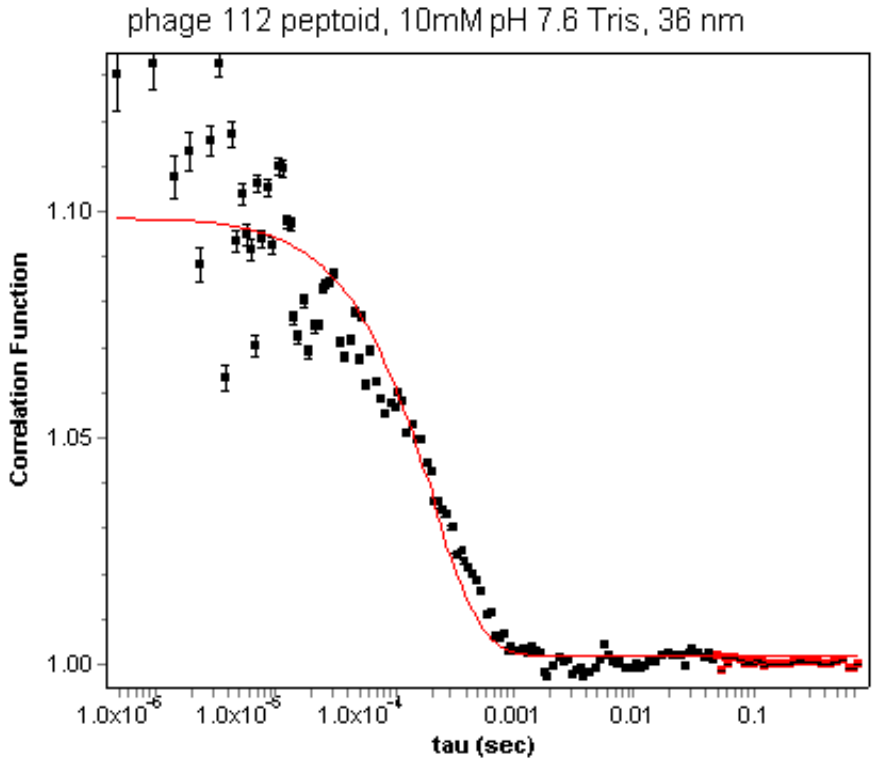

Figure 2-10. Autocorrelation function of dynamic light scattering signal from solution of Phage 112.

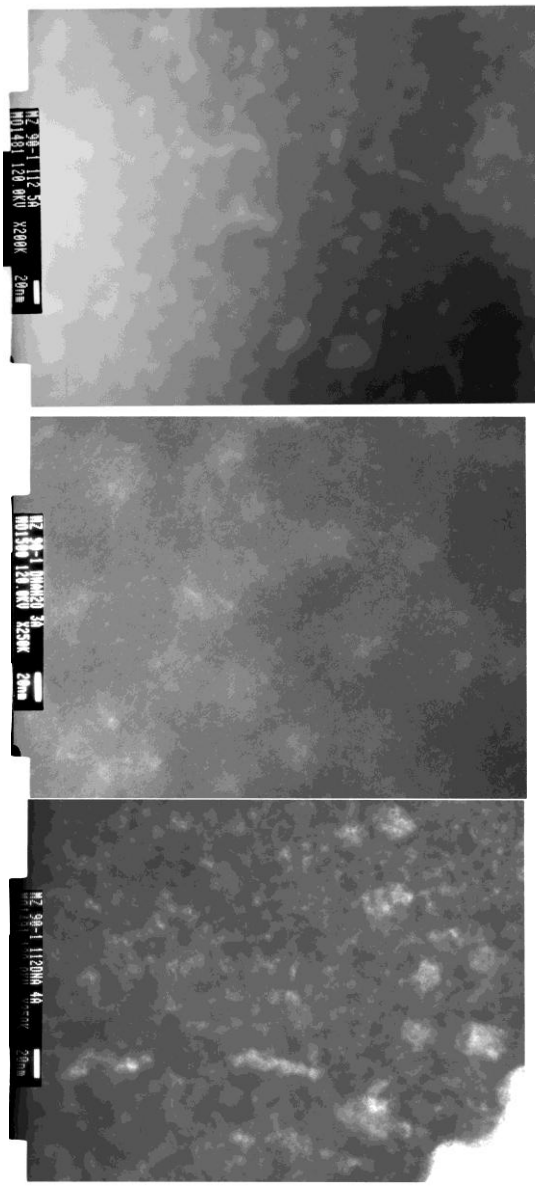

Figure 2-11. Transmission electron micrographs of phage 112 peptoid (top), a single-stranded DNA 30mer (middle), and a mixture of the two (bottom), stained with sodium phosphotungstate. Scale bars are 20 nm.

As a strategy to obtain a phage mimic that will form an aggregate at neutral pH, we sought a neutral hydrophilic sidechain that can substitute for some of the carboxyl groups and increase the net charge on the peptoids at neutral pH. We explored the use of amides, but found that unprotected primary amide sidegroups undergo dehydration reactions during the cleaving step, and that adding protecting groups to α-amino amides is challenging. Instead, we turned to the commercially available chiral *S*-1-methoxy-2-aminopropane, which can form the monomer Nsmp. Methoxy groups are relatively hydrophilic, and peptoids containing them are known to be water-soluble. The *R* enantiomer is not commercially available, and the *S* enantiomer rotates polarized light in the opposite direction from the Nspe sidechain. To determine whether helical

conformations result from the use of Nsmp, we prepared peptoids of the form $(XYNspe)_4$ and $(XYNrpe)_4$ where X and Y are combinations of Nsmp, Nsce, and the achiral methoxyethyl (Nmeo) or carboxymethyl (Ngly). Figure 2-12 shows that some of these show more prominent peaks in their circular dichroism spectra. Note that this was a screening study using crude products, so the abscissa units are approximate and impurities may have influenced these results. Apparently, helicity is preserved with considerable flexibility to add neutral hydrophilic substituents when Nsce is also used, and Nsmp can be used alone or with achiral carboxyl groups with varying results. The peptoids $(Nsmp_2Nspe)_4$ and a version of phage 112 where Nsce is replaced with Nsmp were studied by gel electrophoresis as above.

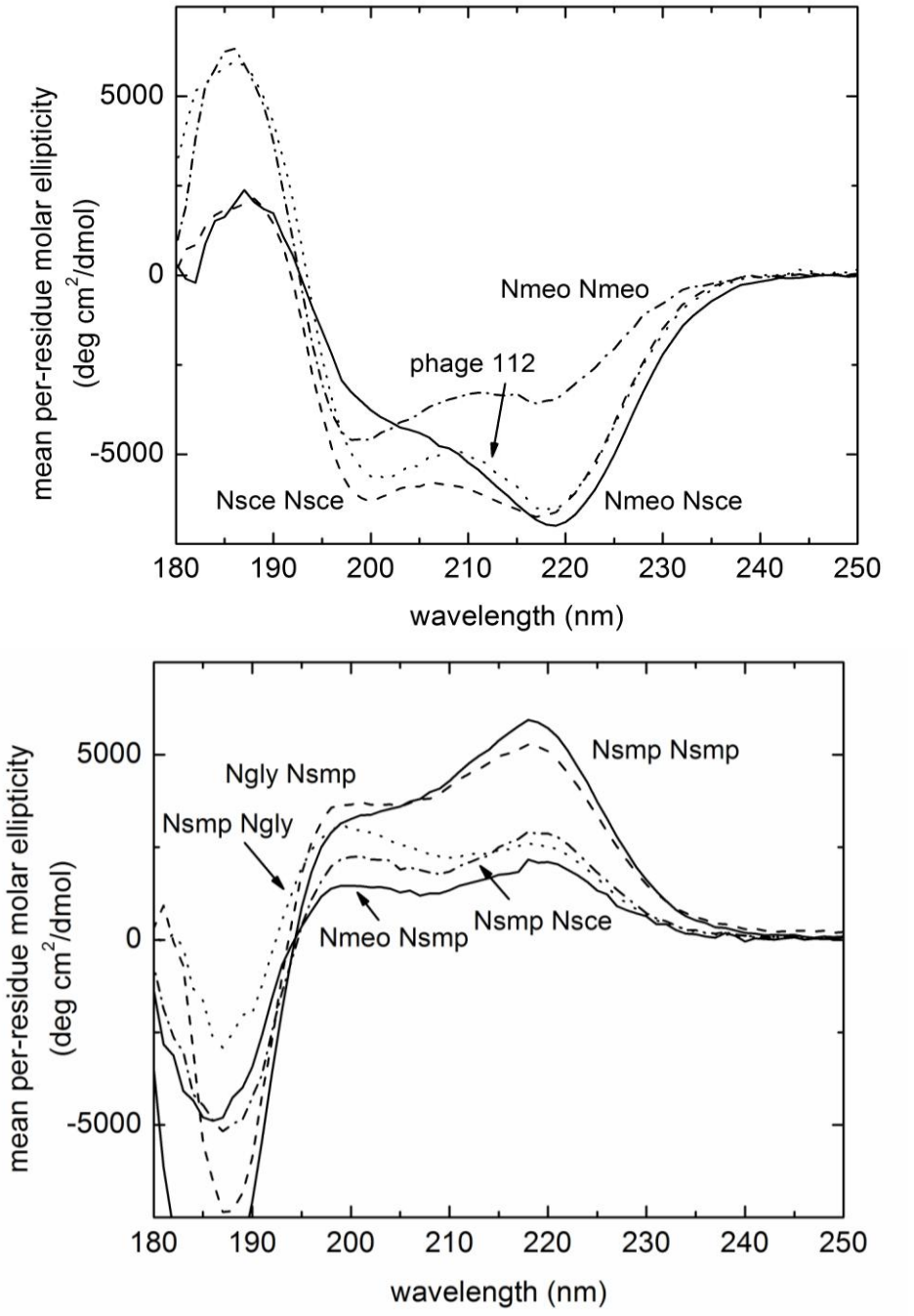

Figure 2-12. Circular dichroism spectra of $(XYNspe)_4$ (top) and $(XYNrpe)_4$ (bottom) where X and Y are the monomers noted in the labels.

As shown in Figure 2-13, an Nsmp-containing peptoid with no cationic sidegroups (and is cationic only at the N terminus) does not interact with DNA, and is either not hydrophobic enough to be stained by Coomassie, or is extracted from the gel during staining. Phage 112-smp interacts with DNA at neutral pH, decreasing the extent to which it binds to ethidium bromide. Excess peptoid appears in the Coomassie stain in the opposite direction from the travel of DNA,

indicating that the peptoid is cationic. Approximately three peptoid molecules were present per DNA base.

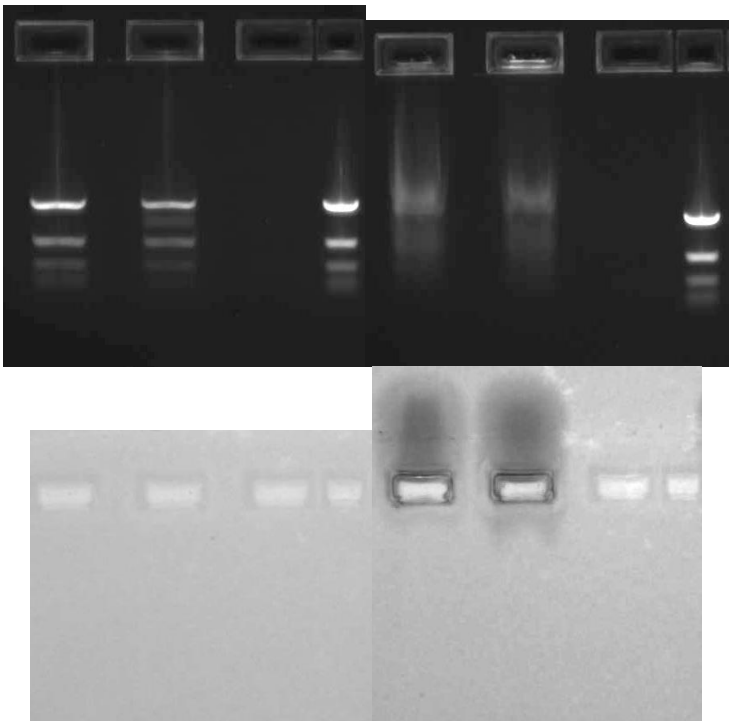

Figure 2-13. Gel electrophoresis of $(Nsmp_2Nspe)_4$ (left) and phage 112-smp (right). Ethidium bromide fluorescence is shown in the top images, and Coomassie-stained gels are on the bottom. In each quadrant, from left to right, are peptoid + DNA ladder, peptoid + DNA ladder at reduced pH, an empty lane, and DNA ladder with no peptoid.

2.6. Summary

We have designed a family of helical peptoids with structural motifs similar to the m13 bacteriophage, and have found that we can tune the interaction of peptoids with double-stranded DNA through variation of the sidegroup sequence. Increasing the number of cationic amine sidegroups from 0 to 2 increases the interaction with DNA, and decreasing the anionic charge by either protonation of carboxylate sidegroups or substitution with neutral hydrophilic sidegroups increases interaction. We have not yet demonstrated formation of rigid filaments, but have observed high aspect ratio aggregates by electron microscopy. Synthesis of longer peptoids – between the 12- and 15mers prepared by us and the approximately 50mers of the bacteriophage coat proteins – may result in more ordered structures that can still be prepared in vitro, and then tested for gene delivery and structural DNA applications.

3. SYNTHESIS OF INORGANIC NANOMATERIALS USING PEPTOIDS

3.1. Introduction

Traditional methods of nanoparticle synthesis generally involve trial-and-error combinations of simple surfactants and inorganic precursors. The future of this field, if it is to reach a stage where nanoscale materials can be rationally designed, will require a greater degree of chemical control of the geometry and mechanism of growth. This is very likely to require the use of sequence-specific polymers. Impressive progress over topological control has been made with DNA, and a large body of knowledge exists on polypeptides, and both are candidates for this task. However, a class of artificial sequence-specific polymers, known as oligo (N-functional glycine)s or peptoids, forms much more stable secondary structures, offers more functional diversity, and is cheaper to synthesize than biopolymers.[14] Specific assembly has been demonstrated, but much work remains to be done to master this. With further work, it is likely that the outstanding properties of peptoids will make them a competitive technology for bottom-up nanomaterial assembly, alone or in conjunction with other sequence-specific polymers.

Our main strategy is to develop peptoids that can form rodlike reverse micelles or cylindrical shell assemblies. Peptoid synthesis was performed at the Molecular Foundry at Lawrence Berkeley Lab, as described in previous chapters, with modifications noted below. Peptoids with chiral aromatic sidegroups are expected to have three monomers per turn.[13] We hypothesized that we could make cylindrical micelles if the first two monomers in a turn have chiral hydrophobic side chains of varying shapes, and the third is a hydrophilic monomer, creating a cross section similar to the AOT molecule discussed in the previous chapter. To obtain control over the length and diameter of the materials, we would then modulate the shape and functionality of the hydrophobic sidegroups to achieve specific inter-peptoid associations. However, filamentous structures can also be synthesized using peptides that have the usual head-to-tail orientation of a surfactant. We synthesized several peptoids in each category and have examined their ability to modulate growth of inorganic nanomaterials.

3.2. Peptoid Synthesis

3.2.1. Axial surfactants; sulfonatoethyl sidegroup

The syntheses of several axial surfactants are described in Chapter 2, including those where amines and carboxylates act as the hydrophilic groups, including an unprotected but sterically hindered amine that can be a cationic group in aqueous solution. We also examined the use of taurine as a means to introduce an unprotected anionic sidegroup with a low pKa. The monomer can be dissolved at 1 M concentrations in N,N-dimethylformamide or N-methylpyrrolidone if it is converted from the zwitterion to the free-base tetraethylammonium salt by dissolving in 1 eq 25% tetraethylammonium hydroxide in methanol. The product is reduced to a viscous oil by rotary evaporation at less than 50 °C, dissolved in either solvent, and used as an ordinary peptoid submonomer. Taurine is attached to the peptoid in high yield. Unfortunately, this monomer inhibits further growth of the peptoid chain. It is believed that this is caused by ion pairing of the sulfonate and the terminal amine under the acidic conditions of bromoacylation. Improved yield

is observed by introduction of high concentrations of added salt, such as lithium bromide or triethylammonium bromoacetate, during each subsequent bromoacylation.

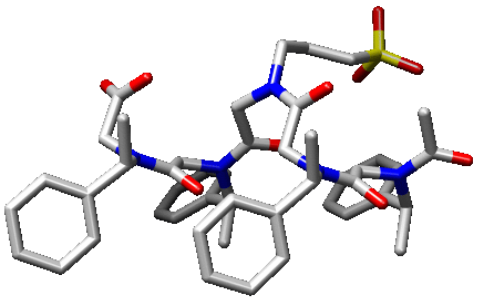

Figure 3-1. Structure of acetyl $Nspe_2$-taurine-$Nspe_2$, a peptoid analog of AOT.

3.2.2. Conventional Surfactants; Zwitterionic and Dicationic Headgroups

Taurine was incorporated at the N terminus of a hydrophobic peptoid such as $Nspe_8$ to create a zwitterionic surfactant, and has been provided to a collaborator for characterization of its properties. Unprotected free-base tetraethylammonium salts of amino acids such as alanine can be added in the same way. Reaction of N,N,N',N'-tetramethyl diaminopropane (P22) as a terminal submonomer results in a quaternary-tertiary dicationic surfactant with properties that we report in greater detail here. Figure 3-1 shows the structure of this peptoid. Addition of quaternary ammonium sidegroups in the middle of the peptoid was attempted – such as a propylpyridinium or trimethylaminoethyl sidegroup – but the quaternary ammonium groups do not survive in high yield when subject to subsequent treatments with high concentrations of primary amines, as occurs in further submonomer additions.

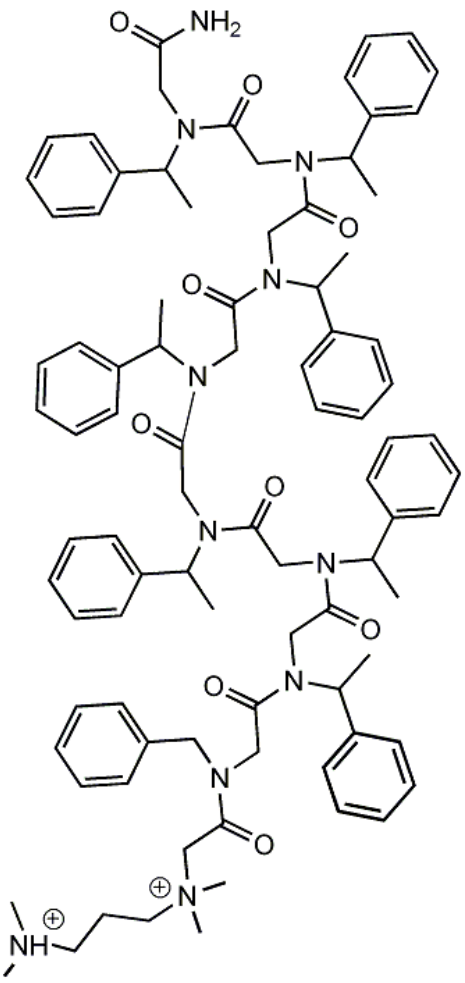

Figure 3-2. Structure of P22-NBz-Nspe$_7$, a dicationic peptoid surfactant.

We performed an initial SANS measurement of a sample of 0.4 wt % P22-NBz-Nspe$_7$ in Na acetate D_2O buffer, pH 5.0, at 20 °C and at 55 °C. The results shown in Figure 3-3 indicate that primary particles are linked up into higher order structures. In Figure 3-4, the data at 56 °C are compared with best fits to models involving a power law combined with the following particle shapes: sphere, cylinder, and core-shell cylindrical micelle. The spherical model is not consistent with the data. Cylinder and core-shell cylinder micellar forms give good agreement with the data in combination with a low-Q power law of roughly 2.4. Ideally, data at lower Q values would establish the characteristics of the higher order aggregate structure.

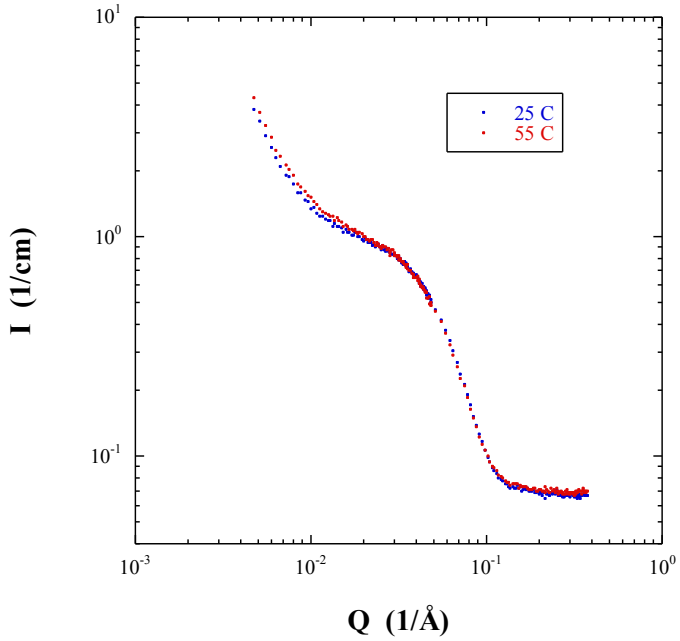

Figure 3-3. Small-angle neutron scattering data collected on a solution of P22-NBz-Nspe$_7$ in sodium acetate D_2O buffer.

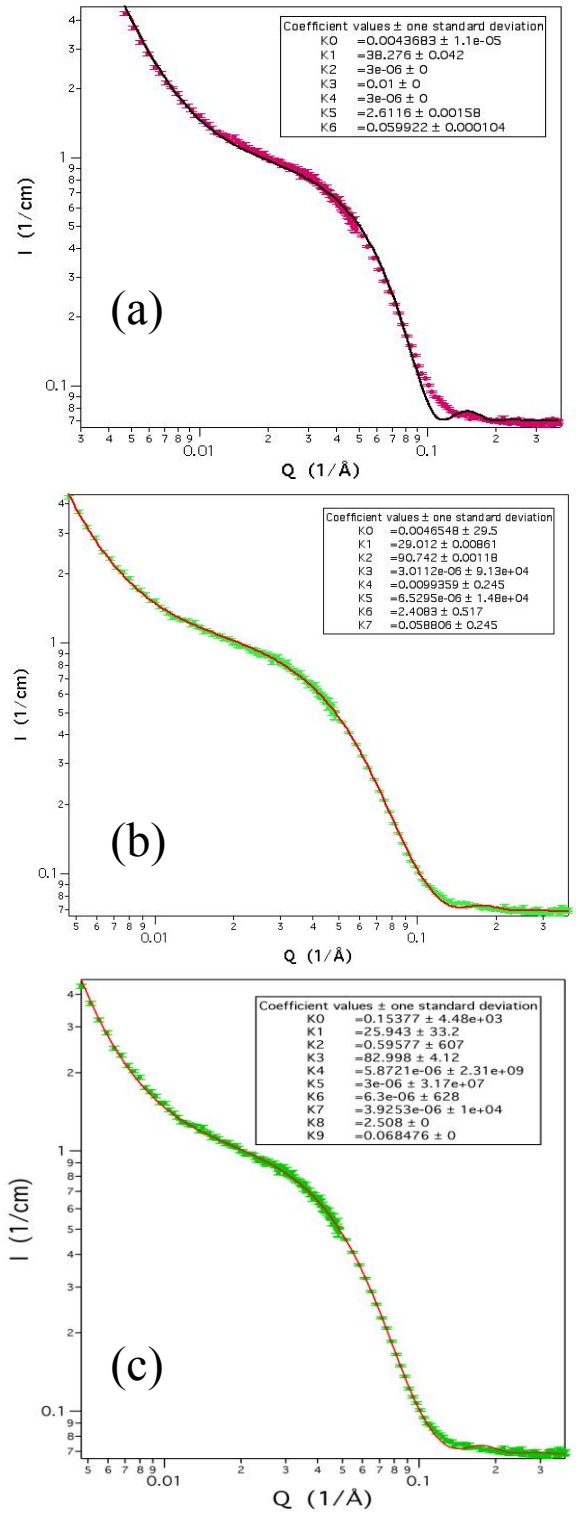

Figure 3-4. Fits of preliminary data to the following models: a) power law + sphere, b) power law + cylinder, c) power law + core-shell cylinder.

Diamine groups are known to catalyze the reaction of silicate, buffered at near-neutral pH, to silica.[47] If the diamines have a micellar structure, we hypothesize that the silica product will, to some extent, conform to the shape of the micelle. To test this, we applied our previously published assay to the peptoid and to surfactants synthesized by methods described in that work, which are shown in Figure 3-5.

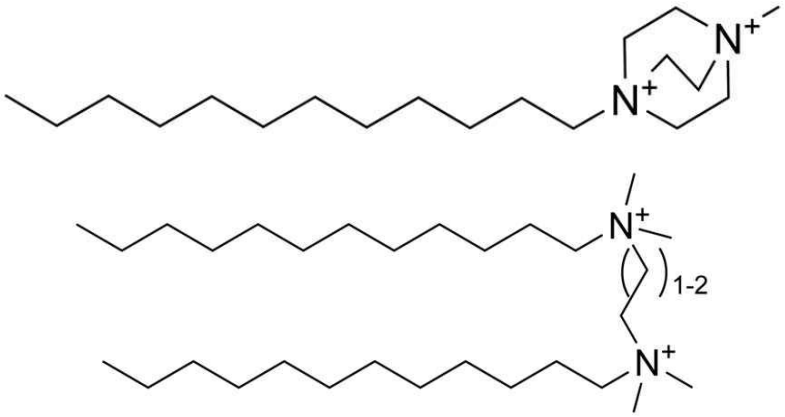

Figure 3-5. Dicationic surfactants used for comparison to the peptoid in Figure 3-4: MeDABCO C12 (top) and $(C12)_2$P22 (bottom).

When these surfactants were mixed with buffered silica at room temperature, a cloudy suspension formed within one minute. The product was cast, rinsed with water, and dried onto a wafer, sputtered with a thin layer of gold-palladium alloy, and imaged with a scanning electron microscope. The products are shown in Figure 3-6.

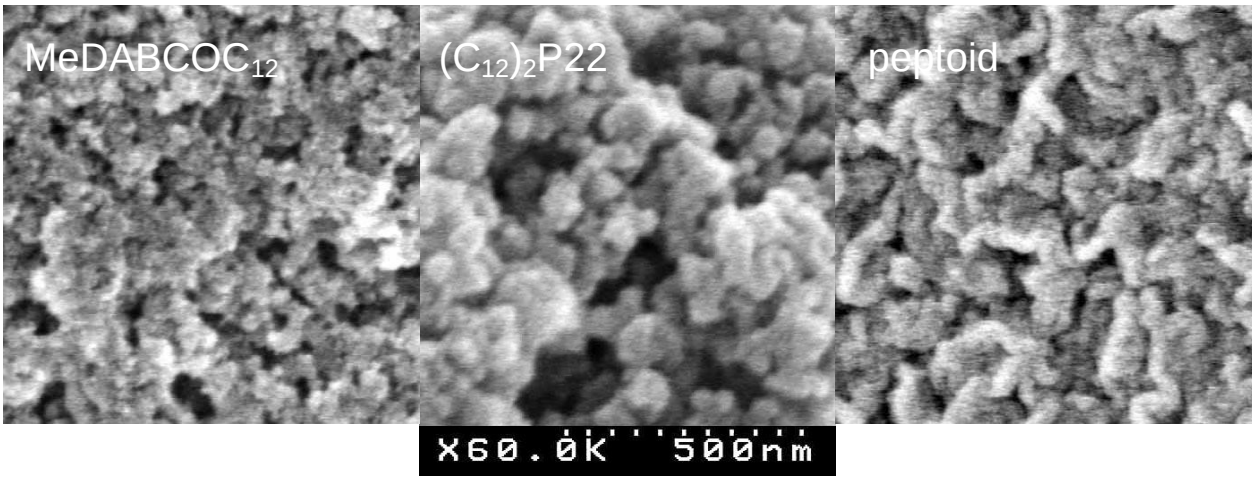

Figure 3-6. Scanning electron micrographs of silica formed using the dicationic surfactants shown in Figures 3-5 and 3-2.

The alkyl surfactants result in aggregates of roughly spherical particles. In contrast, the product produced with the peptoid has tubular or wormlike shapes that are about 50 nm in diameter, suggesting that the ability to modulate the structure of the silica has been obtained.

4. MASS SPECTROMETRY STUDIES OF PEPTOID FRAGMENTATION

4.1. Introduction

Advanced mass spectrometry techniques provide rich information that can be used to confirm the composition and sequence of peptoids. For this, we seek the ability to control fragmentation patterns to ensure that we can predictably and generally determine a structure. We are investigating peptoid fragmentation patterns under different tandem mass spectrometry conditions. We have studied a few model peptoids by using collision-induced dissociation (CID) and infrared multiphoton dissociation (IRMPD) experiments. We have observed rich and characteristic sequence information by fragmenting protonated and alkali metal complexed peptoids. Synthesis of peptoids was by the procedures described in Chapter 2.

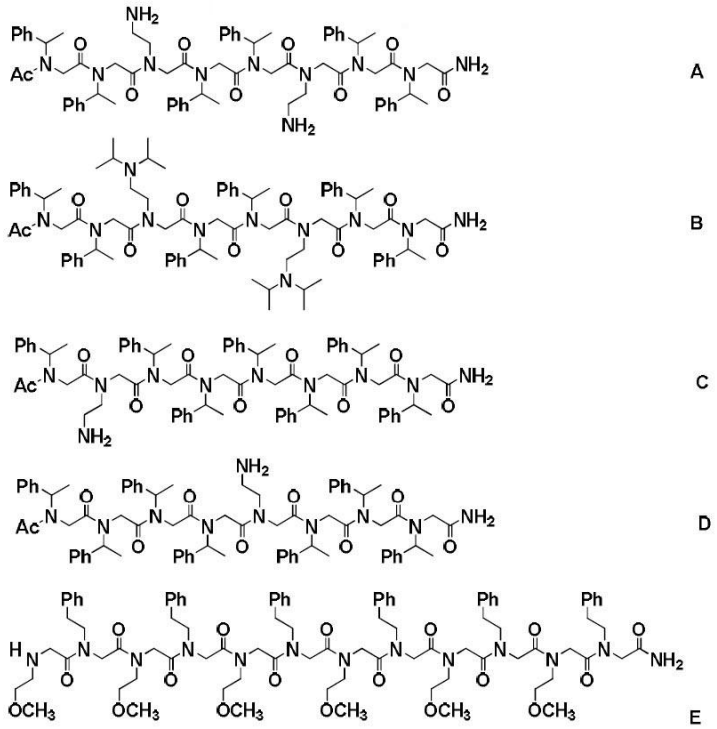

Figure 4-1. Structures of Peptoids A-E as studied by mass spectrometry.

4.2. Mass Spectrometry Experiments

The IRMPD and most CID experiments were performed using a MALDI-LTQ-FTICR instrument (Thermo Fisher Scientific). Some CID experiments were also done with an LTQ linear ion trap (Thermo Fisher) equipped with an AP-MALDI ion source (Mass Tech Inc.). The MALDI samples were prepared as the following. For protonated ions, 1 μL of peptoid solution (10 pg/μL) was spotted, followed by 1 μL of matrix solution of α-Cyano-4-hydroxycinnamic

acid (CHCA) and allowed to air dry. For alkali metal adducts, 1µL of peptoid solution was spotted, followed by 1 µL of a 0.1 M solution of MCl (M = Li, Na, K, Rb, or Cs), and then followed by 1 µL of matrix slution of CHCA.

4.2.1. Collision-Induced Dissociation of Peptoid B

The protonated peptoid B, presumably with a proton on one of the two amines, yields a series of Y-ions (fragments toward the C terminus) with the most abundant ion being Y7. The B-ions (toward the N terminus) are not detected and are most likely not positively charged. The Li^+ and other alkali metal adducts yield both Y-ions and B-ions, with the most abundant fragments at Y6 and B5.

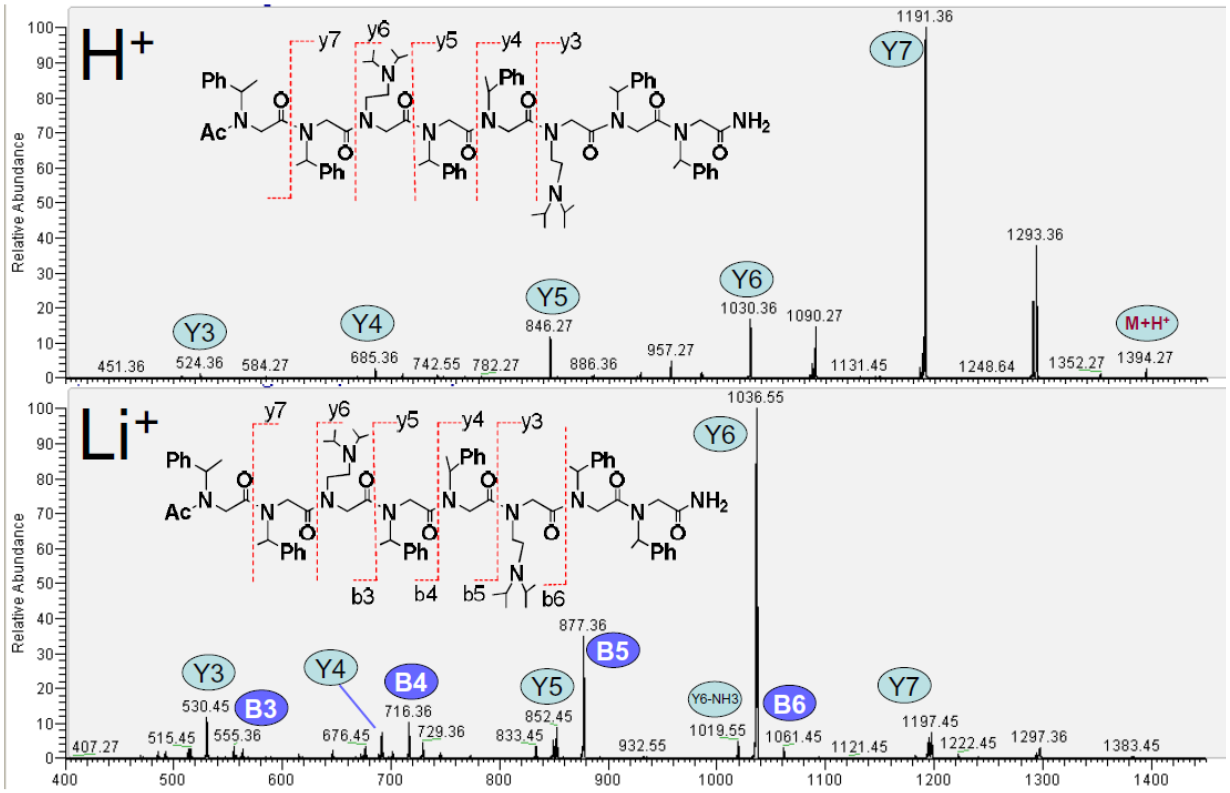

Figure 4-2. Collision-induced dissocation of Peptoid B.

4.2.2. Collision-Induced Dissociation of Peptoid A

The protonated peptoid A fragments to produce a series of Y-ions. The most abundant ion is Y7. The alkali metal adducts of peptoid fragment to produce not only the Y-ions, but also a series of B-ions. The most abundant ions are Y6 and B5. Like peptoid B, peptoid A is amine-containing, and shows similar fragmentation patterns.

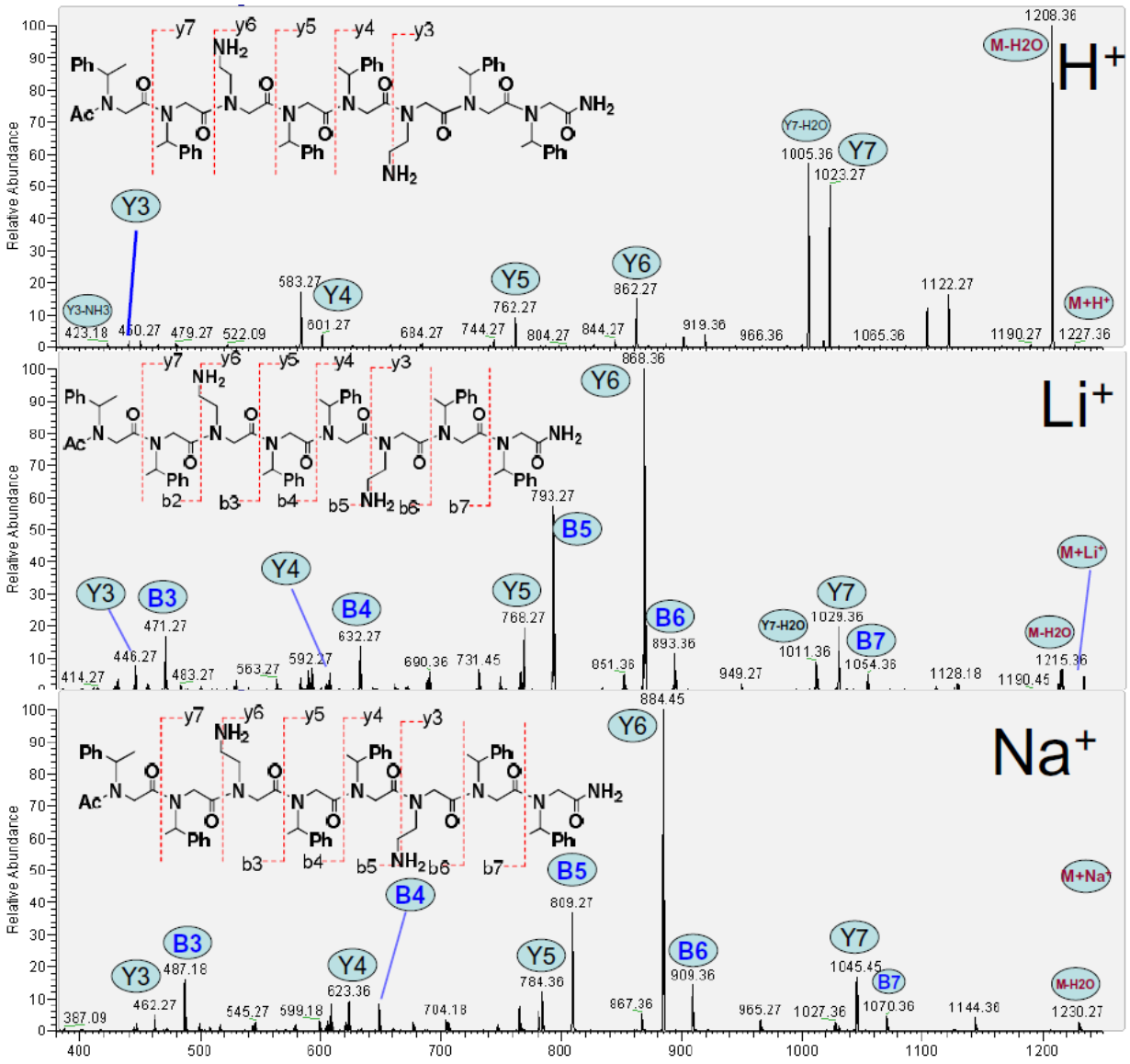

Figure 4-3. Collision-induced dissocation of Peptoid A.

4.2.3. Molecular Modeling of Peptoid A

The geometries of the peptoids were modeled at the AM1 level using Gaussian 03 suite of programs. The results show that both protons and alkali metal ions bind to amines. Protons also hydrogen bond to backbone oxygens, where as alkali metal ions have less selective interactions with the rest of the peptoid. Protonation at N3 results in a globular conformation, and protonation at N6 gives a helix. Lithium (and other alkali metal) addition at both N3 and N6 yield helices.

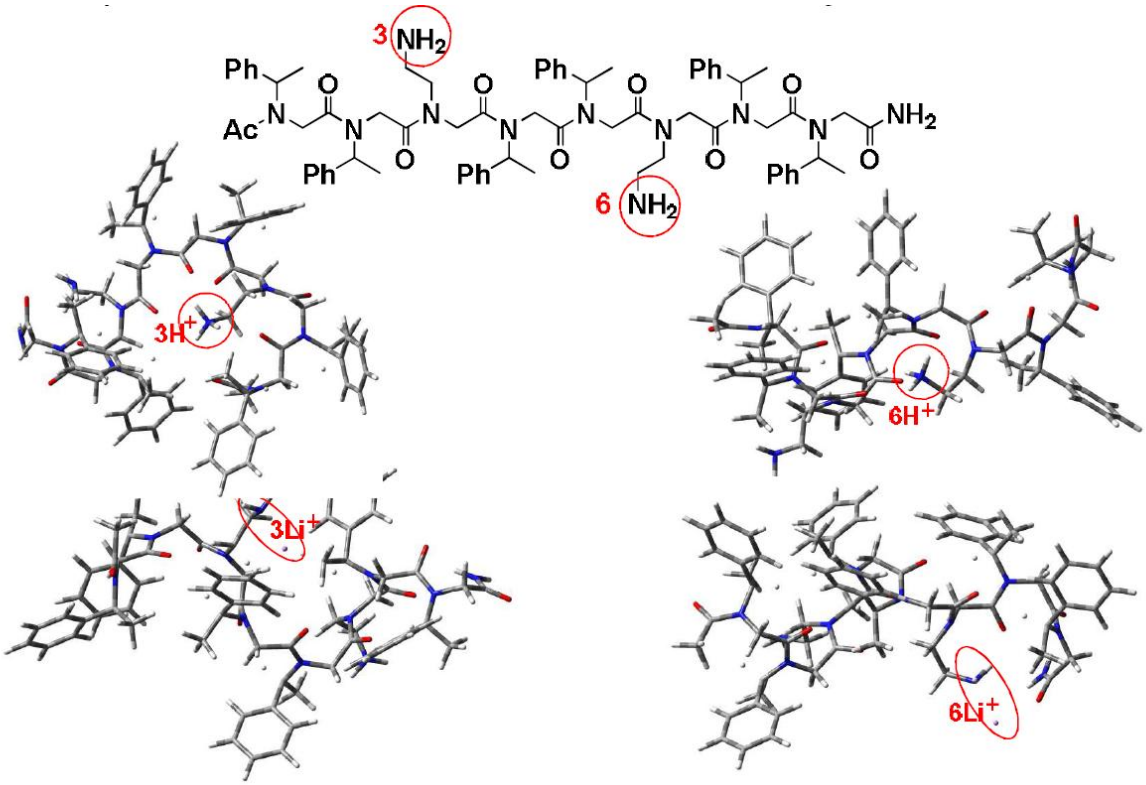

Figure 4-4. Computational models of peptoid A in the presence of cations.

4.2.4. Infrared Multiphoton Dissociation of Peptoid B

The protonated peptoid B yields a series of Y-ions (and again no B-ions) with the most abundant ion of Y3. So, both dissociation methods favor fragmentation near an amine sidegroup. While the Li^+ and other metal adducts yield both Y-ions and B-ions with the most abundant ions at Y3 and B5.

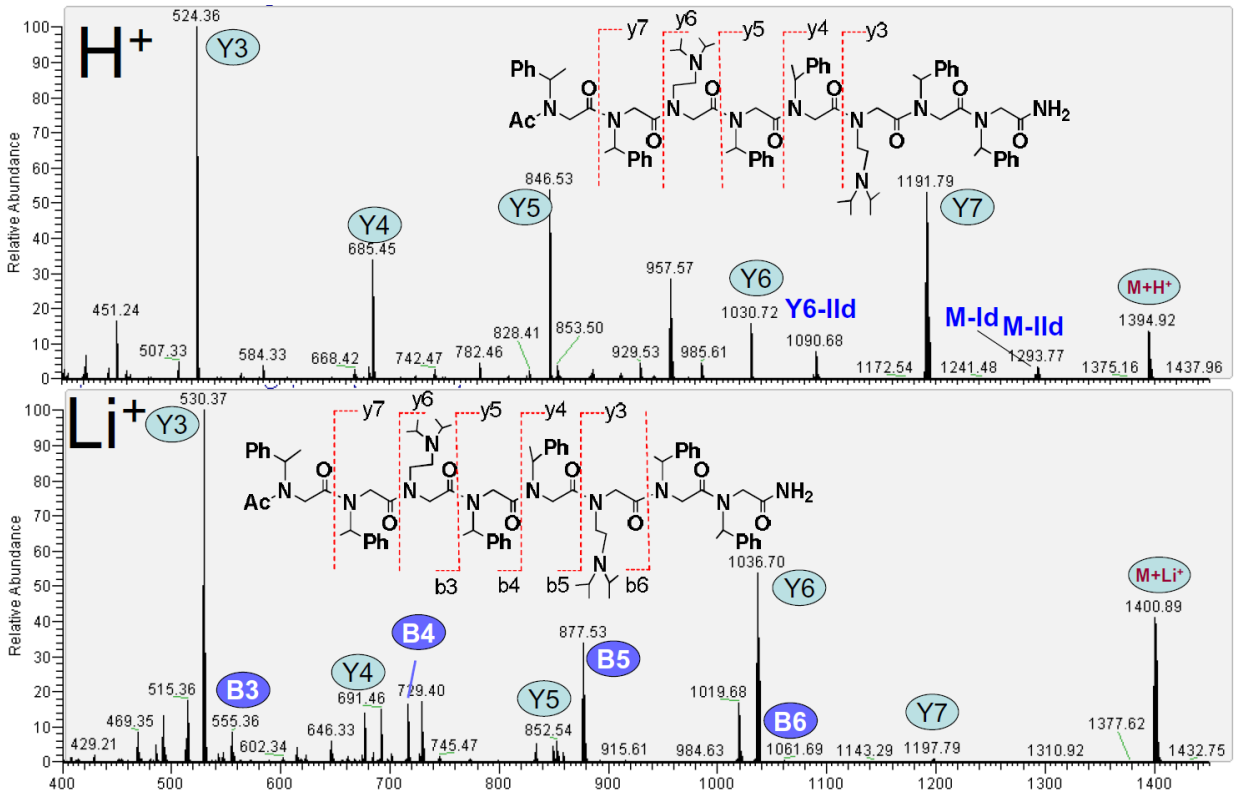

Figure 4-5. Infrared multiphoton dissocation of Peptoid B.

4.2.5. Collision-Induced Dissociation of Peptoid C

The protonated peptoid C yields a series of Y-ions with the most abundant ion of Y7, fragmenting near the amine as before, and yielding no B-ions. In this simpler peptoid, the Li^+ and other alkali metal adducts yield both Y-ions and B-ions with the most abundant fragments at the same fragmentation location, Y7 and B6.

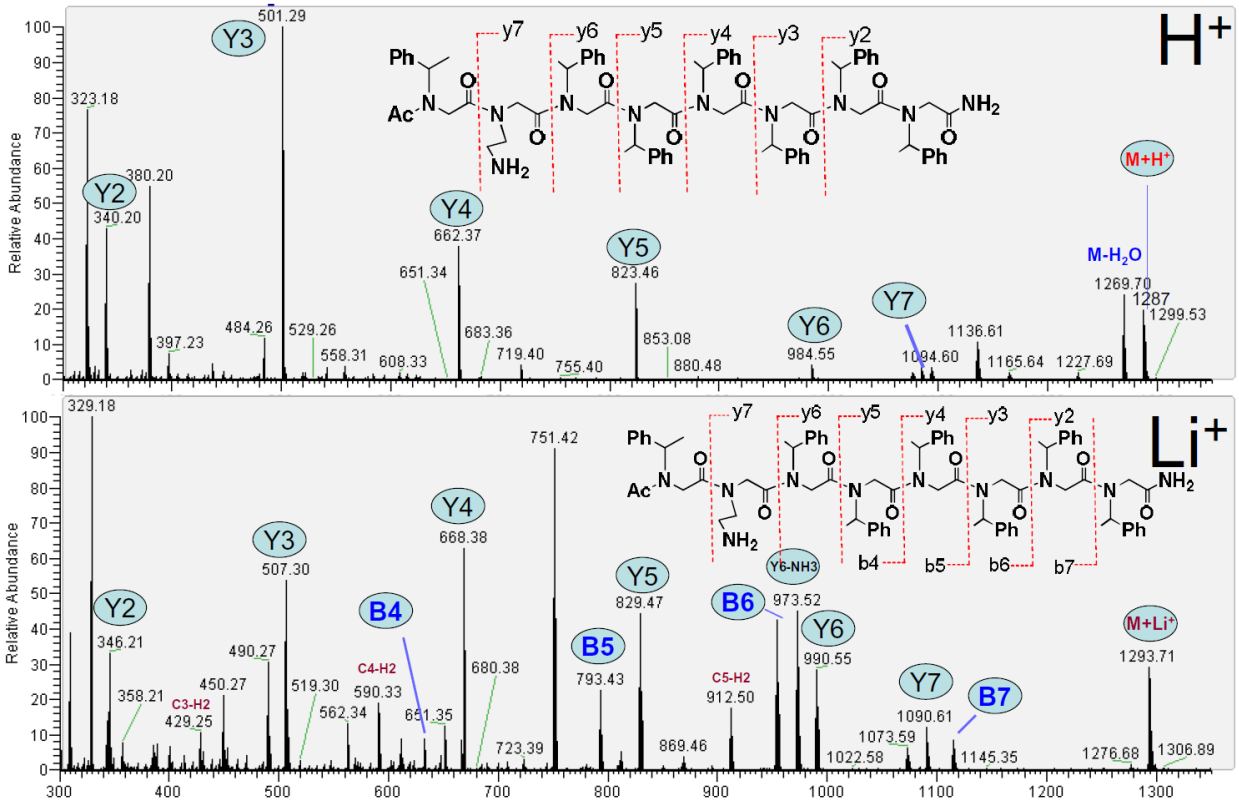

Figure 4-6. Collision-induced dissocation of Peptoid C.

4.2.6. Collision-Induced Dissociation of Peptoid D

The protonated peptoid D has an amine closer to the middle of the peptoid. It yields a series of Y-ions with the most abundant ion being Y7 – preferring to fragment near the end, and not near the amine. While the Li^+ and other alkali metal adducts yield both Y-ions and B-ions with the most abundant fragments near the amine at Y4 and B4. The difference is likely due to differences in conformation, and resulting changes in bond strength and collision sites.

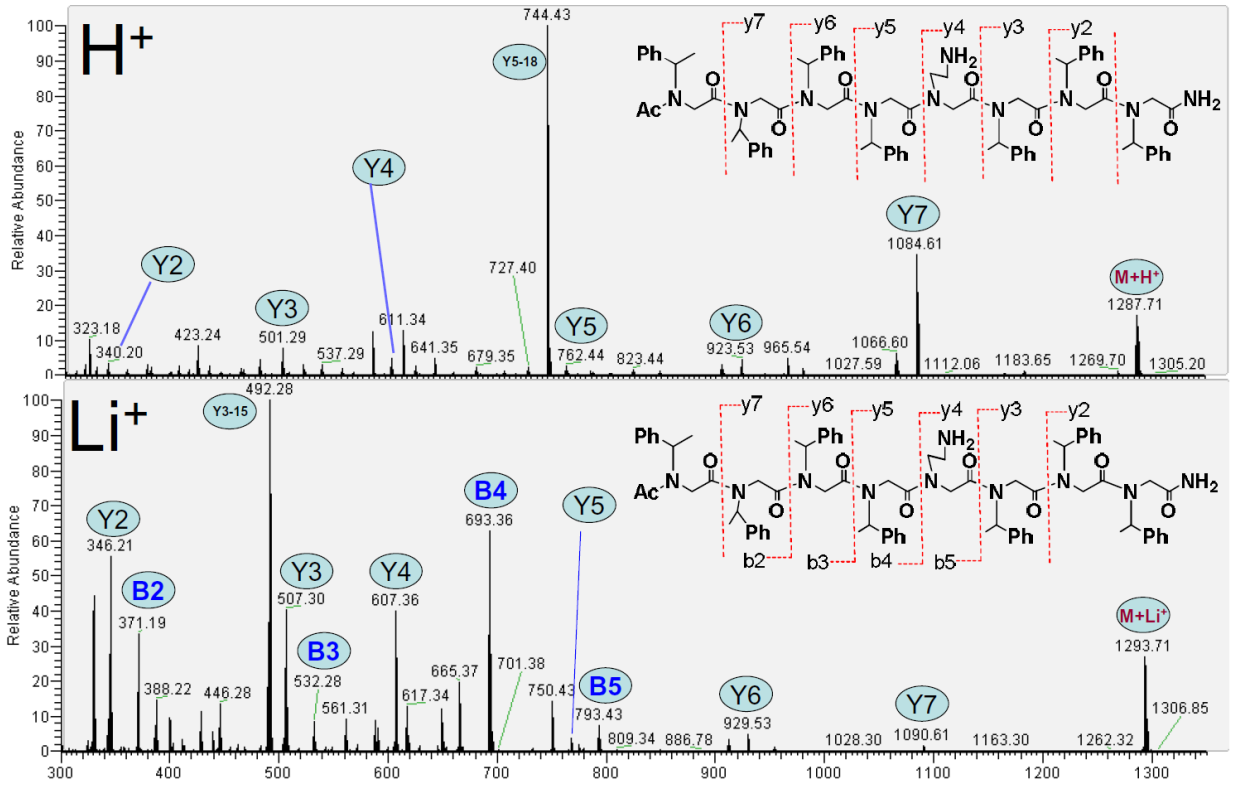

Figure 4-7. Collision-induced dissocation of Peptoid D.

4.2.7. Collision-Induced Dissociation of Peptoid E

Peptoid E has no amine sidegroups, but an amine terminus, and many ether sidegroups available for interaction with cations. The protonated peptoid E yields mostly Y-ions, but some B-ions, with the most abundant ion being Y10. While the Li+ and other alkali metal adducts yield both Y-ions and B-ions with relatively even distributions of ion intensity, consistent with their trend of being less selective.

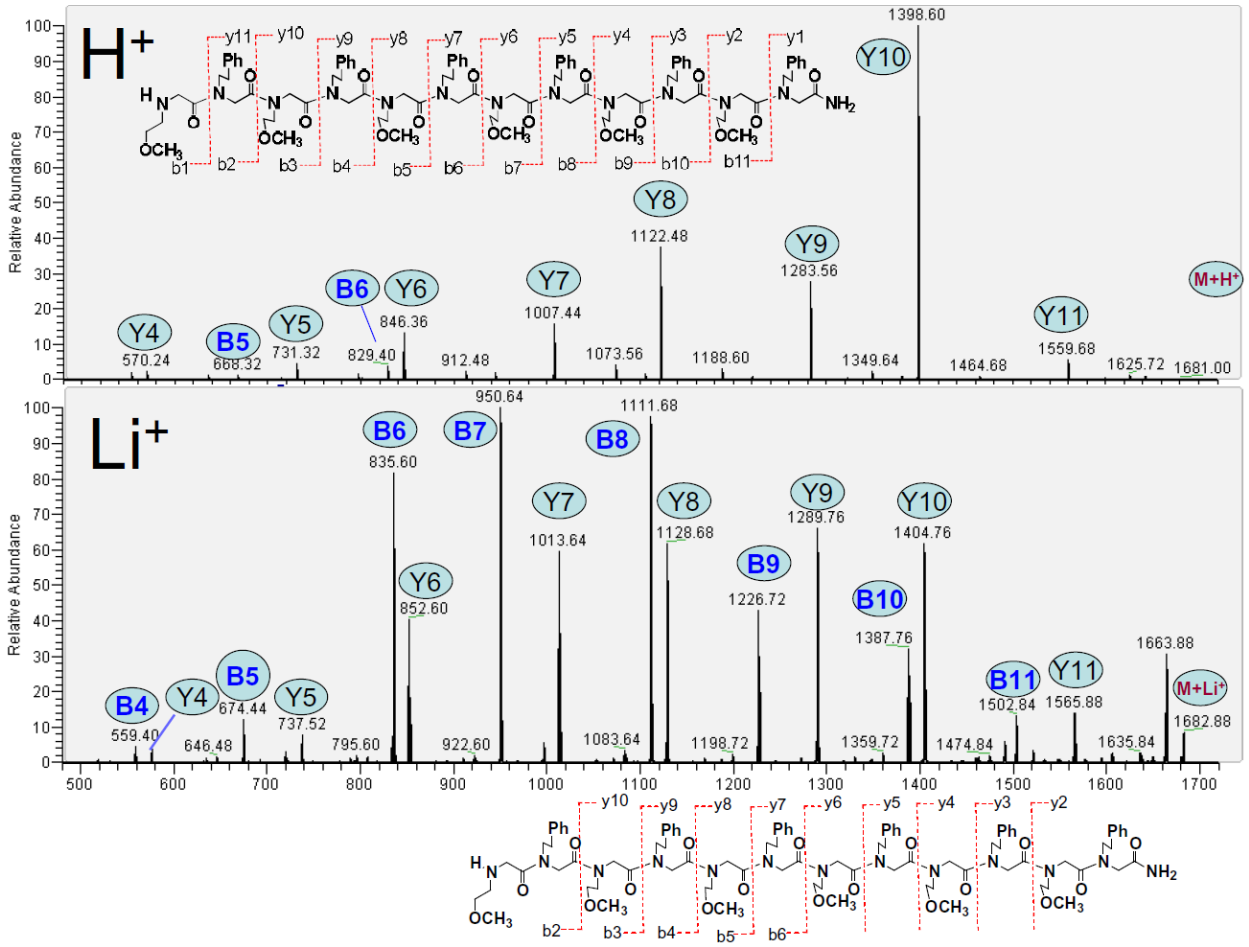

Figure 4-8. Collision-induced dissocation of Peptoid E.

4.2.8. Infrared Multiphoton Dissociation of Peptoid C

The protonated peptoid C yields a series of Y-ions with the most abundant ion of Y3, not near the amine as for collision-induced dissociation. The Li^+ and other metal adducts yield both Y-ions and B-ions with relatively even distributions of the intensity, also not favoring Y7.

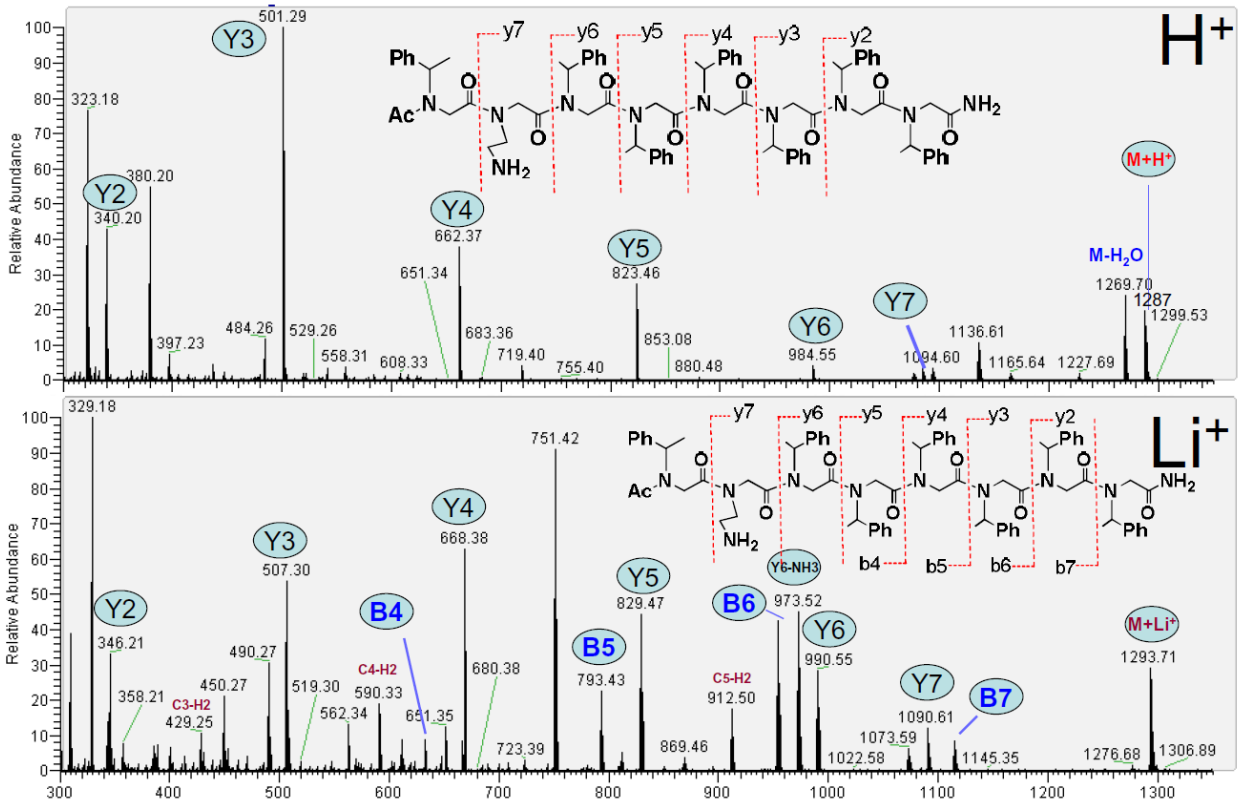

Figure 4-9. Infrared multiphoton dissocation of Peptoid C.

4.2.9. Infrared Multiphoton Dissociation of Peptoid D

The protonated peptoid D yields a series of Y-ions with the most abundant ions being Y7 and Y5-18. The Li^+ and other metal adducts yield both Y-ions and B-ions with the most abundant ions being Y3-15 and B4, suggesting lower specificity for the amine.

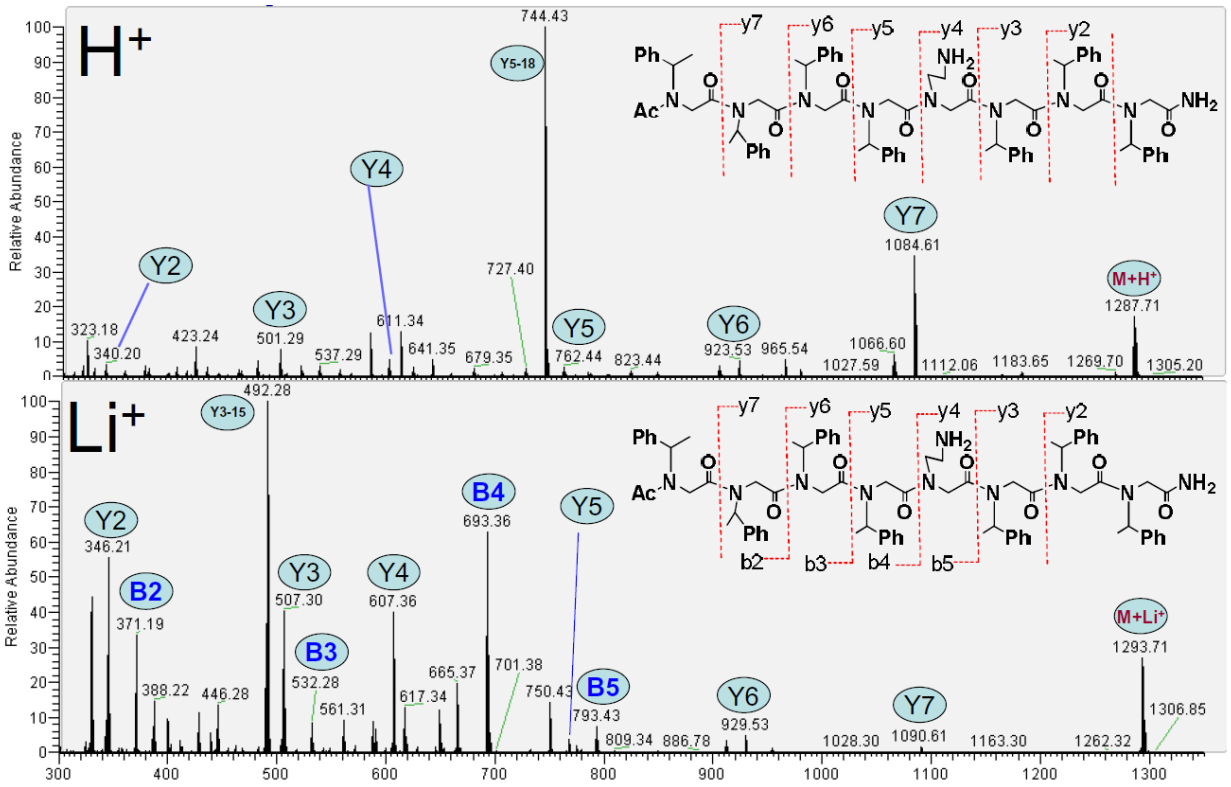

Figure 4-10. Infrared multiphoton dissocation of Peptoid D.

4.2.10. Infrared Multiphoton Dissociation of Peptoid E

The protonated peptoid E yields mostly Y-ions, but some B-ions, with relatively even distribution of ion intensity. While the Li+ and other alkali metal adducts yield both Y-ions and B-ions with the most abundant ion being B6.

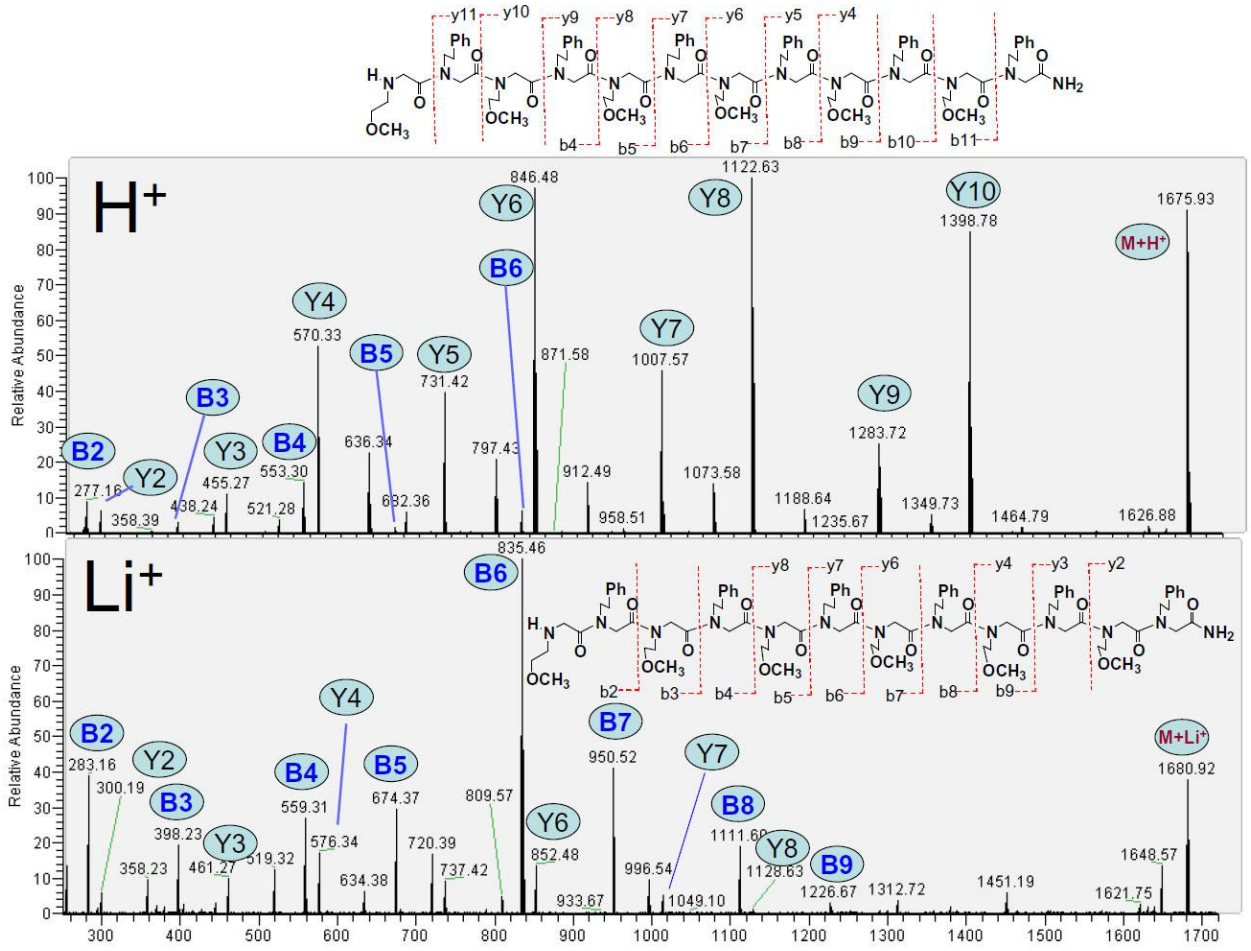

Figure 4-11. Infrared multiphoton dissocation of Peptoid E.

4.3. Conclusion

The fragmentation patterns of peptoids are complex, and depend on the binding site of the cation, the resulting conformation, and the fragmentation mechanism. The conformations and fragmentation patterns using protons as the cations are generally more specific, favor amine sidegroups and/or the N-terminus, and yield mostly or exclusively fragments on the C-terminal side. Alkali metal cations are less selective, affording a broader distribution of ions that may aid sequence determination. Infrared multiphoton dissociation tends to be less selective than collision-induced dissociation. Combinations of these techniques provide an array of valuable evidence that can be used to obtain confidence in determination of the structure of peptoid samples.

9. REFERENCES

1. Nykypanchuk, D.; Maye, M. M.; van der Lelie, D.; Gang, O. Nature 2008, 451, 549-552.
2. Mao, C. D.; Sun, W. Q.; Seeman, N. C. Nature 1997, 386, 137-138.
3. Schlick, T. L.; Ding, Z. B.; Kovacs, E. W.; Francis, M. B. J. Am. Chem. Soc. 2005, 127, 3718-3723.
4. McMillan, R. A.; Paavola, C. D.; Howard, J.; Chan, S. L.; Zaluzec, N. J.; Trent, J. D. Nature Mater. 2002, 1, 247-252.
5. Mao, C. B.; Solis, D. J.; Reiss, B. D.; Kottmann, S. T.; Sweeney, R. Y.; Hayhurst, A.; Georgiou, G.; Iverson, B.; Belcher, A. M. Science 2004, 303, 213-217.
6. Wang, Z. C.; Medforth, C. J.; Shelnutt, J. A. J. Am. Chem. Soc. 2004, 126, 15954-15955.
7. Seeman, N. C.; Belcher, A. M. Proc. Nat. Acad. Sci. 2002, 99, 6451-6455.
8. Knez, M.; Bittner, A. M.; Boes, F.; Wege, C.; Jeske, H.; Maiss, E.; Kern, K. Nano Lett 2003, 3, 1079-1082.
9. Rabin, O.; Herz, P. R.; Lin, Y. M.; Akinwande, A. I.; Cronin, S. B.; Dresselhaus, M. S. Adv. Funct. Mater. 2003, 13, 631-638.
10. Doshi, D. A.; Gibaud, A.; Goletto, V.; Lu, M. C.; Gerung, H.; Ocko, B.; Han, S. M.; Brinker, C. J. J. Am. Chem. Soc. 2003, 125, 11646-11655.
11. Braun, P. V.; Osenar, P.; Tohver, V.; Kennedy, S. B.; Stupp, S. I. J. Am. Chem. Soc. 1999, 121, 7302-7309.
12. Drzaic, P.; Chiang, A.; Stewart, R.; Hermanns, A.; Shi, Y.; Jacobsen, J. J. Soc. Info. Display 2003, 11, 81-87.
13. Armand, P.; Kirshenbaum, K.; Falicov, A.; Dunbrack, R. L.; Dill, K. A.; Zuckermann, R. N.; Cohen, F. E. Folding & Design 1997, 2, 369-375.
14. Burkoth, T. S.; Beausoleil, E.; Kaur, S.; Tang, D. Z.; Cohen, F. E.; Zuckermann, R. N. Chem. & Bio. 2002, 9, 647-654.
15. Lee, B. C.; Zuckermann, R. N.; Dill, K. A. J. Am. Chem. Soc. 2005, 127, 10999-11009.
16. Zeng, H.; Li, J.; Liu, J. P.; Wang, Z. L.; Sun, S. H. Nature 2002, 420, 395-398.
17. Sau, T. K.; Murphy, C. J. Langmuir 2004, 20, 6414-6420.
18. Simmons, B. A.; Li, S. C.; John, V. T.; McPherson, G. L.; Bose, A.; Zhou, W. L.; He, J. B. Nano Lett. 2002, 2, 263-268.
19. Attard, G. S.; Bartlett, P. N.; Coleman, N. R. B.; Elliott, J. M.; Owen, J. R.; Wang, J. H. Science 1997, 278, 838-840.
20. Butler, P. J. G. Phil. Trans. Roy. Soc. London Ser. B-Bio. Sci. 1999, 354, 537-550.
21. Stubbs, G. Rep. Prog. Phys. 2001, 64, 1389-1425.
22. Marvin, D. A.; Hale, R. D.; Nave, C.; Citterich, M. H. J. Mol. Bio. 1994, 235, 260-286.
23. Smith, G. P.; Petrenko, V. A. Chem. Rev. 1997, 97, 391-410.
24. Park, S.; Lee, D. H.; Xu, J.; Kim, B.; Hong, S. W.; Jeong, U.; Xu, T.; Russell, T. P. Science 2009, 323, 1030-1033.
25. Robinson, D. B.; Persson, H. H. J.; Zeng, H.; Li, G. X.; Pourmand, N.; Sun, S. H.; Wang, S. X. Langmuir 2005, 21, 3096-3103.
26. Tao, Y. F.; McCulloch, B.; Kim, S.; Segalman, R. A. Soft Matter 2009, 5, 4219-4230.
27. Long, J. W.; Dunn, B.; Rolison, D. R.; White, H. S. Chem. Rev. 2004, 104, 4463-4492.
28. Huang, Y.; Chiang, C. Y.; Lee, S. K.; Gao, Y.; Hu, E. L.; De Yoreo, J.; Belcher, A. M. Nano Lett. 2005, 5, 1429-1434.

29. Knez, M.; Sumser, M.; Bittner, A. M.; Wege, C.; Jeske, H.; Martin, T. P.; Kern, K. Adv. Funct. Mater. 2004, 14, 116-124.
30. Kehoe, J. W.; Kay, B. K. Chem. Rev. 2005, 105, 4056-4072.
31. Klug, A. Phil. Trans. Roy. Soc. London Ser. B-Bio. Sci. 1999, 354, 531-535.
32. Wickner, W.; Killick, T. Proc. Nat. Acad. Sci. 1977, 74, 505-509.
33. Marvin, D. A.; Welsh, L. C.; Symmons, M. F.; Scott, W. R. P.; Straus, S. K. J. Mol. Bio. 2006, 355, 294-309.
34. Roth, T. A.; Weiss, G. A.; Eigenbrot, C.; Sidhu, S. S. J. Mol. Bio. 2002, 322, 357-367.
35. Oneil, K. T.; Degrado, W. F. Science 1990, 250, 646-651.
36. Figliozzi, G. M.; Goldsmith, R.; Ng, S. C.; Banville, S. C.; Zuckermann, R. N. In Combinatorial Chem., 1996, p 437-447.
37. Sanborn, T. J.; Wu, C. W.; Zuckerman, R. N.; Barron, A. E. Biopolymers 2002, 63, 12-20.
38. Wu, C. W.; Sanborn, T. J.; Huang, K.; Zuckermann, R. N.; Barron, A. E. J. Am. Chem. Soc. 2001, 123, 6778-6784.
39. Seurynck, S. L.; Patch, J. A.; Barron, A. E. Chem. & Bio. 2005, 12, 77-88.
40. Wu, C. W.; Sanborn, T. J.; Zuckermann, R. N.; Barron, A. E. J. Am. Chem. Soc. 2001, 123, 2958-2963.
41. Wu, C. W.; Kirshenbaum, K.; Sanborn, T. J.; Patch, J. A.; Huang, K.; Dill, K. A.; Zuckermann, R. N.; Barron, A. E. J. Am. Chem. Soc. 2003, 125, 13525-13530.
42. Murphy, J. E.; Uno, T.; Hamer, J. D.; Cohen, F. E.; Dwarki, V.; Zuckermann, R. N. Proc. Nat. Acad. Sci. 1998, 95, 1517-1522.
43. Huang, C. Y.; Uno, T.; Murphy, J. E.; Lee, S.; Hamer, J. D.; Escobedo, J. A.; Cohen, F. E.; Radhakrishnan, R.; Dwarki, V.; Zuckermann, R. N. Chem. & Bio. 1998, 5, 345-354.
44. Jungmann, R.; Liedl, T.; Sobey, T. L.; Shih, W.; Simmel, F. C. J. Am. Chem. Soc. 2008, 130, 10062.
45. Rothemund, P. W. K. Nature 2006, 440, 297-302.
46. Yang, H.; McLaughlin, C. K.; Aldaye, F. A.; Hamblin, G. D.; Rys, A. Z.; Rouiller, I.; Sleiman, H. F. Nature Chem. 2009, 1, 390-396.
47. Robinson, D. B.; Rognlien, J. L.; Bauer, C. A.; Simmons, B. A. J. Mater. Chem. 2007, 17, 2113-2119.

DISTRIBUTION

1	David B. Robinson		8651 (electronic copy)
1	Michael S. Kent		8622 (electronic copy)
1	Bernadette A. Hernandez-Sanchez		1815 (electronic copy)
1	Blake A. Simmons		8630 (electronic copy)
1	MS0899	Technical Library	9536 (electronic copy)
1	MS0123	D. Chavez, LDRD Office	1011


Sandia National Laboratories